Sol-Gel derived Ferroelectric Thin Films for Voltage Tunable Applications

Arne Lüker, Jena, 7. Juli 2009

arnelueker@aim.com

and What is Cranfield University?

Contents

Part 1

- What are Ferroelectrics?
- The Discovery of Ferroelectricity
- Review of Ferroelectric Perovskites
- The non-linear Response of Ferroelectrics
- Different Loss Mechanisms

Part 2

- (Ba, Sr)TiO_3: Preparation, Characterisation and Problems
- (Pb, Sr)TiO_3 50/50: Preparation, Characterisation and Applications
- Mn doped (Pb, Sr)TiO_3 60/40: Characterisation and Phenomena
- (Pb, Sr)TiO_3 directly on SiO_2

Part 3

- Conclusions

What are Ferroelectrics?

Piezoelectricity:

- Paul and Jacques Curie ~1880
- generation of electricity as a result of mechanical pressure and vice versa.

Pyroelectricity:

- Ancient Greeks in tourmaline
- Sir David Brewster 1824
- spontaneous polarization whose amplitude changes under the influence of a temperature gradient.

Ferroelectricity:

- Joseph Valasek 1920 in Rochelle Salt(*)
- direction of polarisation can be reoriented by application of an electric field.

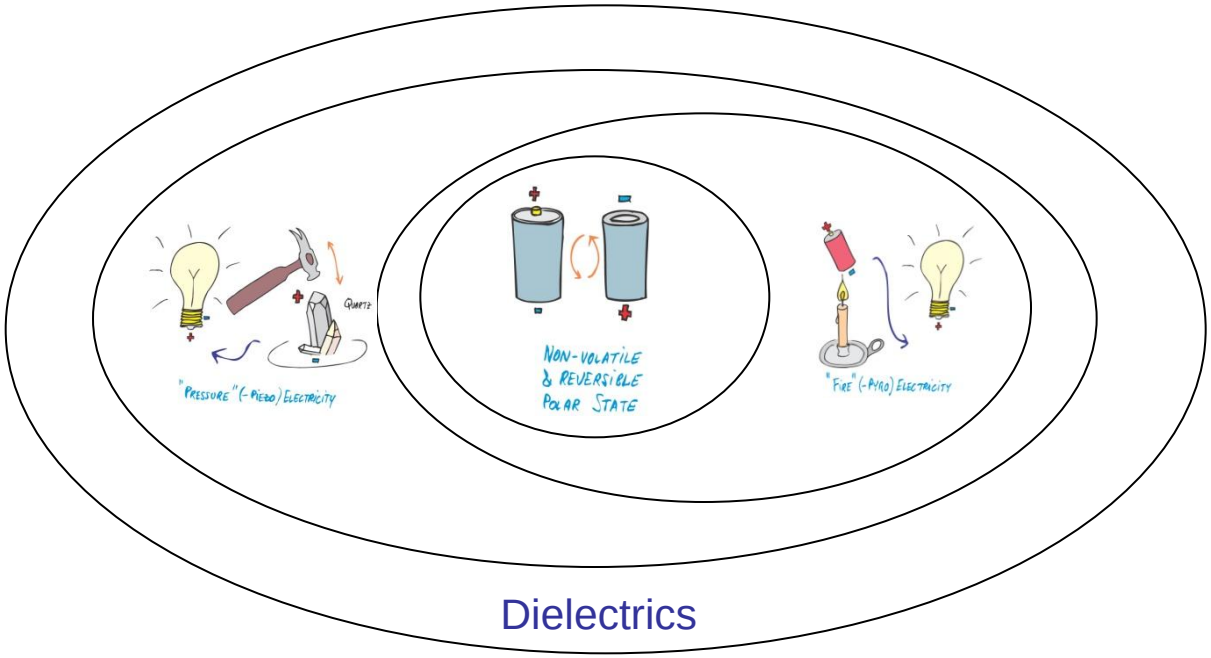

(*) Rochelle Salt, or “sel polychreste” derived from the greek *πολυχρηστοσ,* invented by Elie Seignette as a mild purgative in 1665 in La Rochelle, France.

The Discovery of Ferroelectricity: Joseph Valasek

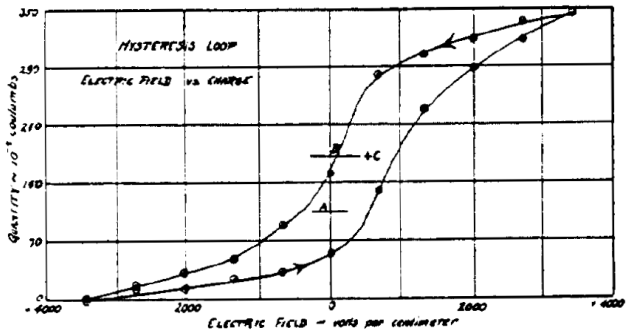

The first published hysteresis curve

"Piezoelectric and allied Phenomena in Rochelle salt", meeting of the American Physical Society in Washington in April **1920**: The data …"*is due to a hysteresis in P analogous to magnetic hysteresis. This would suggest a* ***parrallelism*** *between the behavior of Rochelle salt as a dielectric and steel as a ferromagnetic substance".*

Joseph Valasek 1922

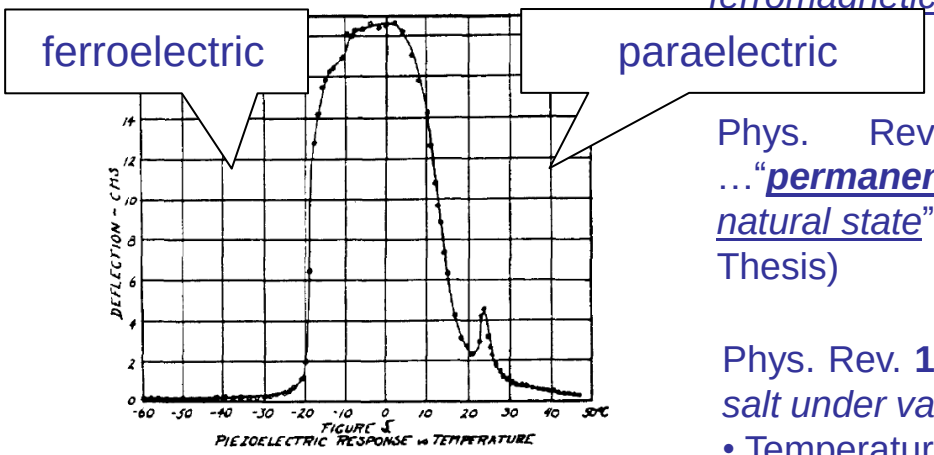

Piezoelectric activity of Rochelle salt vs. temperature indicates the existence of two phase transitions

Phys. Rev. **15**, 537 (**1920**): …"***permanent polarisation*** *is the natural state*" of Rochelle salt. (Master Thesis)

Phys. Rev. **19**, 478-491 (**1922**); "*Piezo-electric activity of Rochelle salt under various conditions*" (Ph.D Thesis).

- Temperature dependence of piezoelectric response
- narrow temperature range of high piezoelectric activity
- indicating the existence of **phase transitions** (Curie Point)

$BaTiO_3$ - the first man-made ferroelectric perovskite , 1942

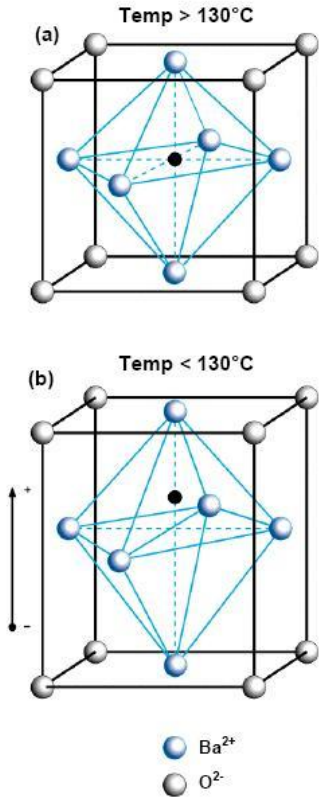

$BaTiO_3$ crystal structure above (a) and below (b) the phase transition between cubic and tetragonal

Goldschmidt's Tolerance Factor

$$t = \frac{r_A + r_O}{\sqrt{2}\left(r_B + r_O\right)}$$

The perovskite structure is stable for:

$$0.75 \le t \le 1$$

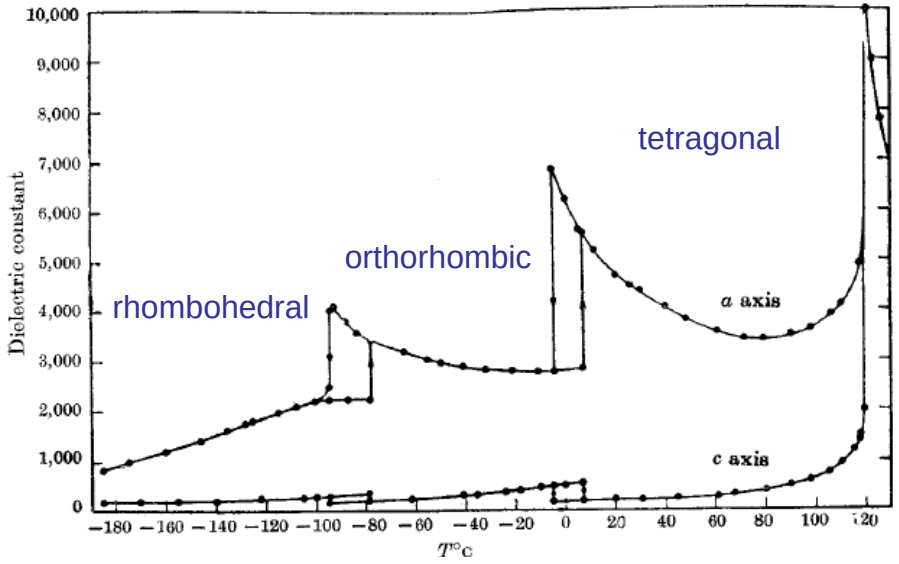

Dielectric constant vs Temperaure of $BaTiO_3$,, Merz 1949 .

Spontaneous Polarisation:

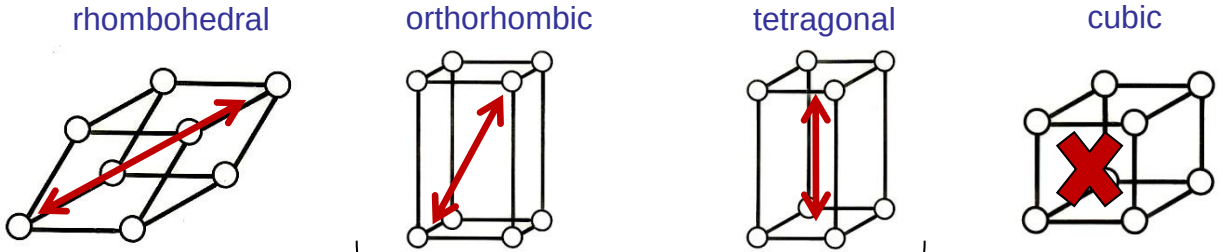

antiferroelectric*)

ferroelectric

paraelectric

*)In an antiferroelectric, unlike a ferroelectric, the total, macroscopic spontaneous polarisation is zero, since the adjacent dipoles cancel each other out

$(Ba,Sr)TiO_3$ – the Shift of the Curie Temperature, 1946

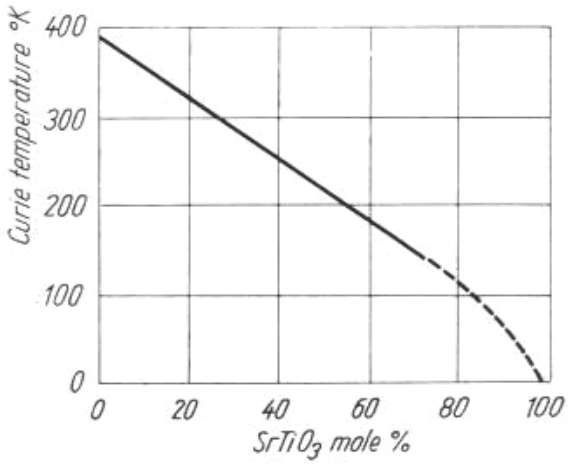

Temperature of phase transition in solid solution of (Ba, Sr)TiO3 vs. composition (Rushman and Strivens, 1946)

- By substituting the the A-site atom (Ba-atom) with Sr the Curie temperature, T_C, can be shifted down from 130°C to around room temperature .
- The linear drop of T_C is ca. 3.4°C per mol%.

Realisation of the paraelectric state at and below room temperature.

Attractive candidate for voltage tunable devices like varactors, phase shifters, DRAMs etc., where the ferroelectric crystal or thin film should be in the paraelectric state viz. the **operating temperature should be above T_C**

Landau-Theory

The Theory of the non-linear Response of Ferroelectrics

$$F = \frac{\alpha}{2}P^2 + \frac{\beta}{4}P^4 + \frac{\gamma}{6}P^6 - EP$$

$$\frac{\partial F}{\partial P} = 0 \Longrightarrow E = \alpha P + \beta P^3 + \gamma P^5$$

$$E = \alpha_0 (T - T_0) P + \beta P^3 + \gamma P^5$$

F: Helmholtz free energy
P: macroscopic polarization
E: macroscopic electric field
α: Temp. dep. material constant
β, γ: Material constant
$T_0 \sim T_C$

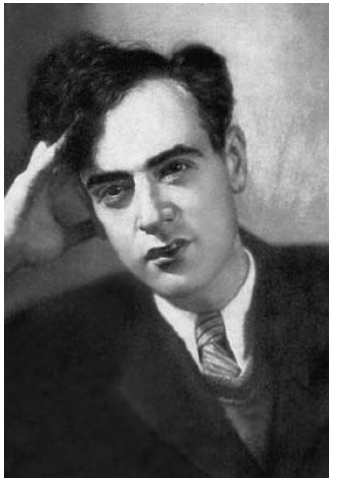

Lew Dawidowitsch Landau

With E=V/d, P=Q/A: $$V = \frac{\alpha(T)d}{A}Q + \frac{\beta d}{A^3}Q^3$$

For a Zero Bias Field:

$$C_{\max} = \left.\frac{dQ}{dV}\right|_{V=Q=0} = \frac{A}{\alpha(T)d} = \frac{\varepsilon 0(T)A}{d}$$

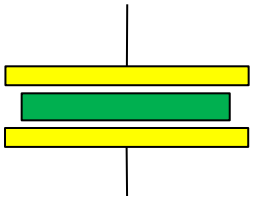

A: Area
D: Distance
Q: Charge
V: Applied Voltage

With ε0(T)=1/α(T) the temperature dependent dielectric permittivity at zero bias

Tunability

The Theory of the non-linear Response of Ferroelectrics – non-zero bias field

$$n = \frac{C_{\max}}{C_{\min}} \quad \text{or} \quad n(\%) = \frac{C_{\max} - C_{\min}}{C_{\max}} \cdot 100$$

It can be shown that the voltage dependent Capacitance can be expressed as:

$$C(V) = \frac{C_{\max}}{\cosh\left[\frac{2}{3}\sinh^{-1}\left(\frac{2V}{V_2}\right)\right] - 1}.$$

Where V_2 is the applied Voltage where $C(V)=C_{max}/2$.

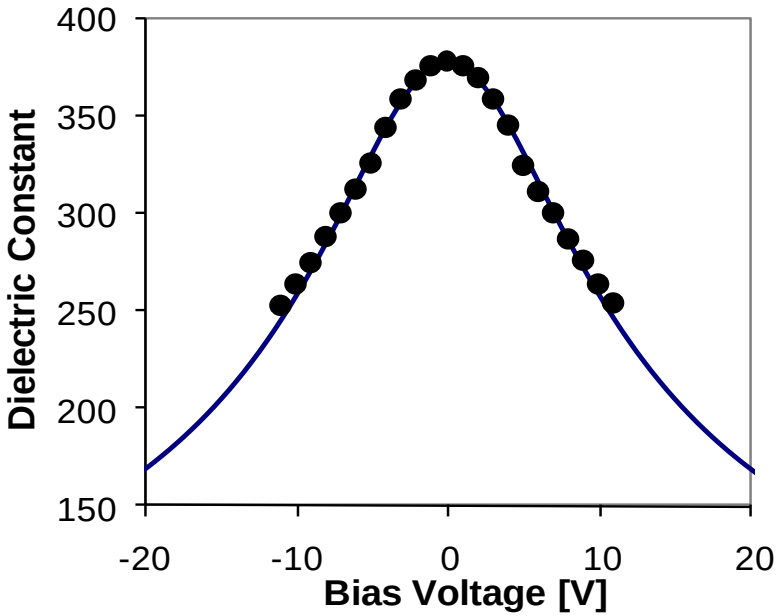

Theoretical curve of the dielectric response (blue) compared to measured values of PST 50/50

Loss

There are different kind of loss mechanisms:

A) Extrinsic loss

General in Films:

- Defects and particles in the film

Due to Measurement (and High Frequencies)

- Electrode loss due to the skin depth
- Fringing fields and parasitic capacitances
- Substrate loss

B) Intrinsic Loss (Solid State Physics)

- Three-Quantum Mechanism (1): *the energy quantum of the electromagnetic field ,ħω, is absorbed during the collision with two thermal phonons*
- Four-Quantum Mechanism (2): *ħω is absorbed during the collision with three phonons*
- Quasi-Debye Loss Mechanism (3): *relaxation of the phonon distribution function (only in the ferroelectric state)*[*)]

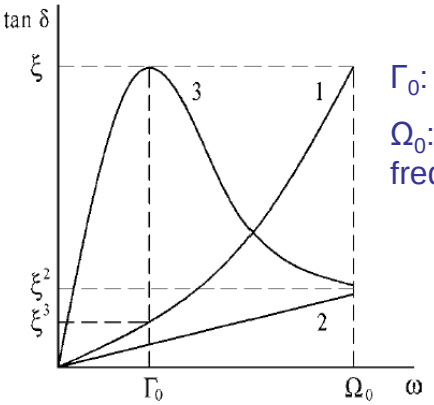

Γ_0: Damping ~ 100 GHz

Ω_0: Soft-mode frequency

Low frequency:

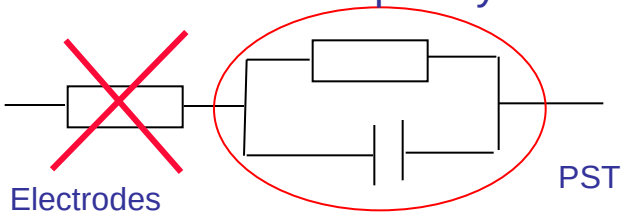

$$\tan\delta = \frac{1}{\omega CR}, \omega \to 0, \tan\delta \to \infty$$

High frequency:

Skin depth:

At 10 GHz:

Al: 814 nm

Cu: 660 nm

Au: 789 nm

Ag: 640 nm

$$\delta = \sqrt{\frac{1}{\pi f \mu_0 \sigma}}$$

Rule of thumb: 3-5 skin depths make electrons happy!

[*)] N. Setter et al.; Polar Ceramics in RF-MEMS and Microwave Reconfigurable Electronics: A Brief Review on Recent Issues; Journal of Electroceramics, 13, 215-222, 2004

Part II

$(Ba, Sr)TiO_3$

- Sol-Gel Synthesis
- Characterisation and Problems

$(Pb, Sr)TiO_3$

- PST 50/50, Preparation, Characterisation and Application
- Mn doped PST 60/40, Characterisation
- Oxygen Vacancies and Electron Hopping
- Enhanced Tunability and Ferroelectricity

$(Pb, Sr)TiO_3$ on SiO_2

- Atomistic Model
- Auger Analysis

$(Ba,Sr)TiO_3$ – Sol-Gel Preparation

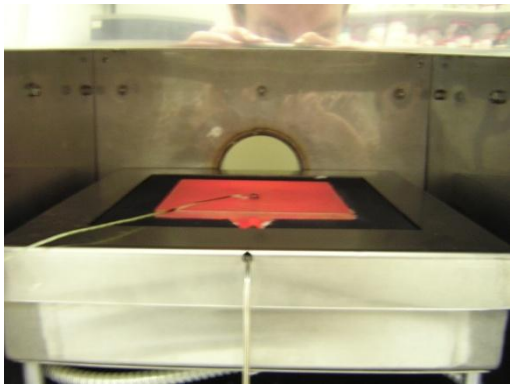

Barium acetate

Strontium acetate

Acetic acid

Titanium Butoxide

2 h stirring

Ethylene Glycol

Precursor Solution

Spin coating (30 sec @ 3000 rpm)

Prebake (2 min @ 330 °C)

Bake (5 min @ 600 °C)

Annealing (10 min @ 700 °C)

BST Thin Film

X-ray Analysis – The Crystallisation of BST

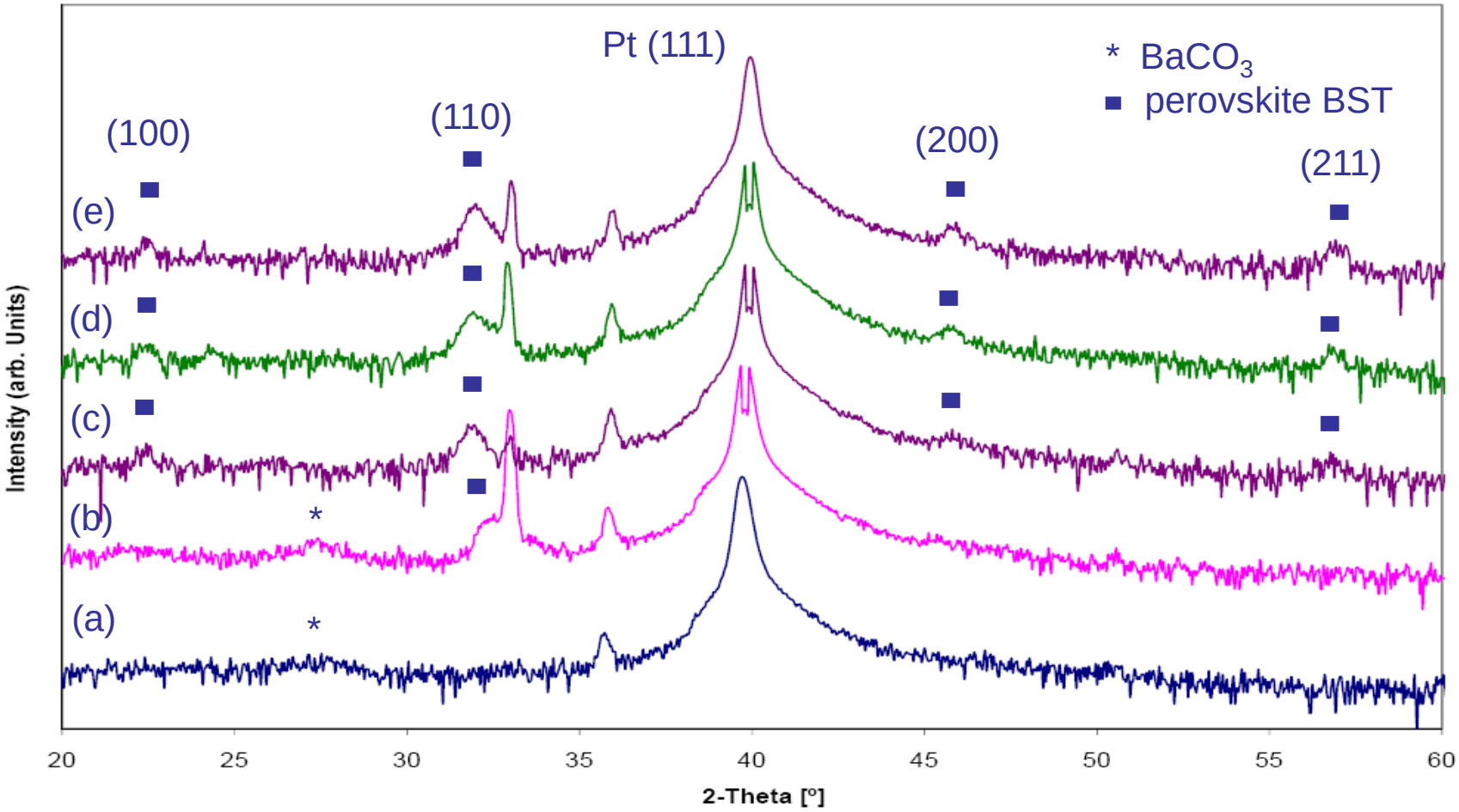

X-ray diffractograms of BST (a) pyrolised at 550°C; annealed at (b) 600°C, (c) 700°C, (d) 800°C, and (e) 900°C for 30 minutes.

Dielectric Properties of BST 60/40

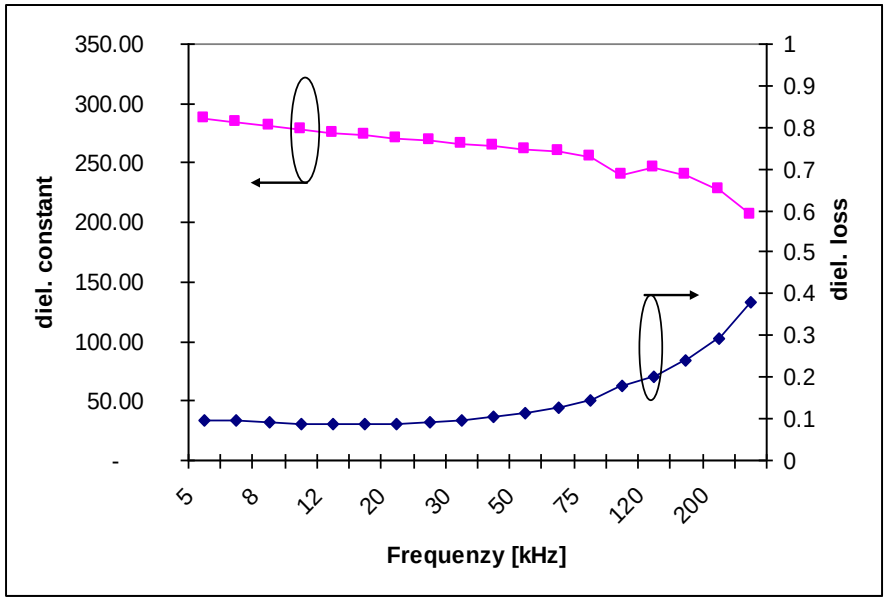

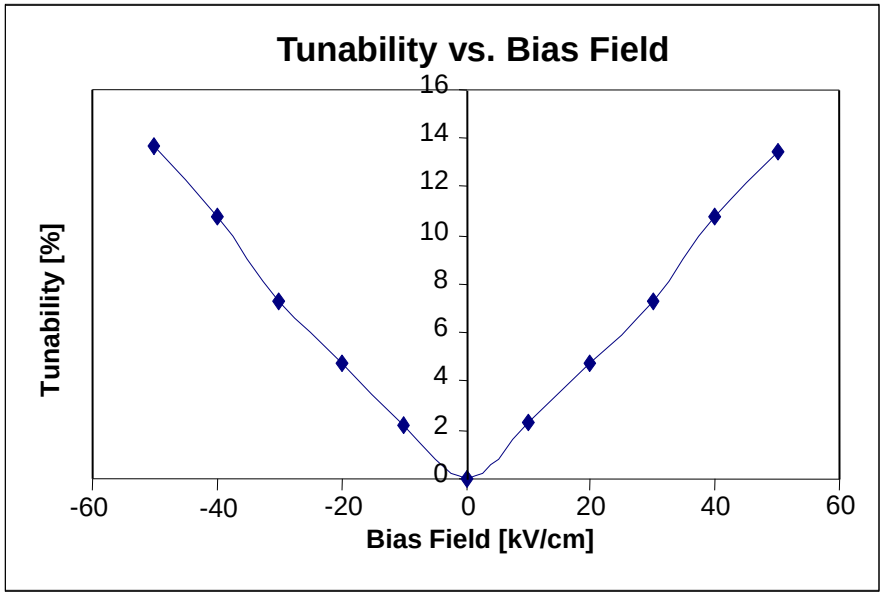

- High losses above 200 kHz (30-40%)
- Tunability ~14% @ 50 kV/cm

Film	Diel. Const.	tanδ	Tunability	K –factor*)
Pure BST50	**2714**	**0.0215**	**51.87**	**24.08**
BST50:MgO	1277	0.0052	28.48	55.12

Room temperature dielectric properties of the pure and heterostructured BST:MgO films measured at 1MHz and applied electric field of 25.3 kV/cm . Jain et al.

*)K-Factor = tunability/loss

Cracks – a major problem

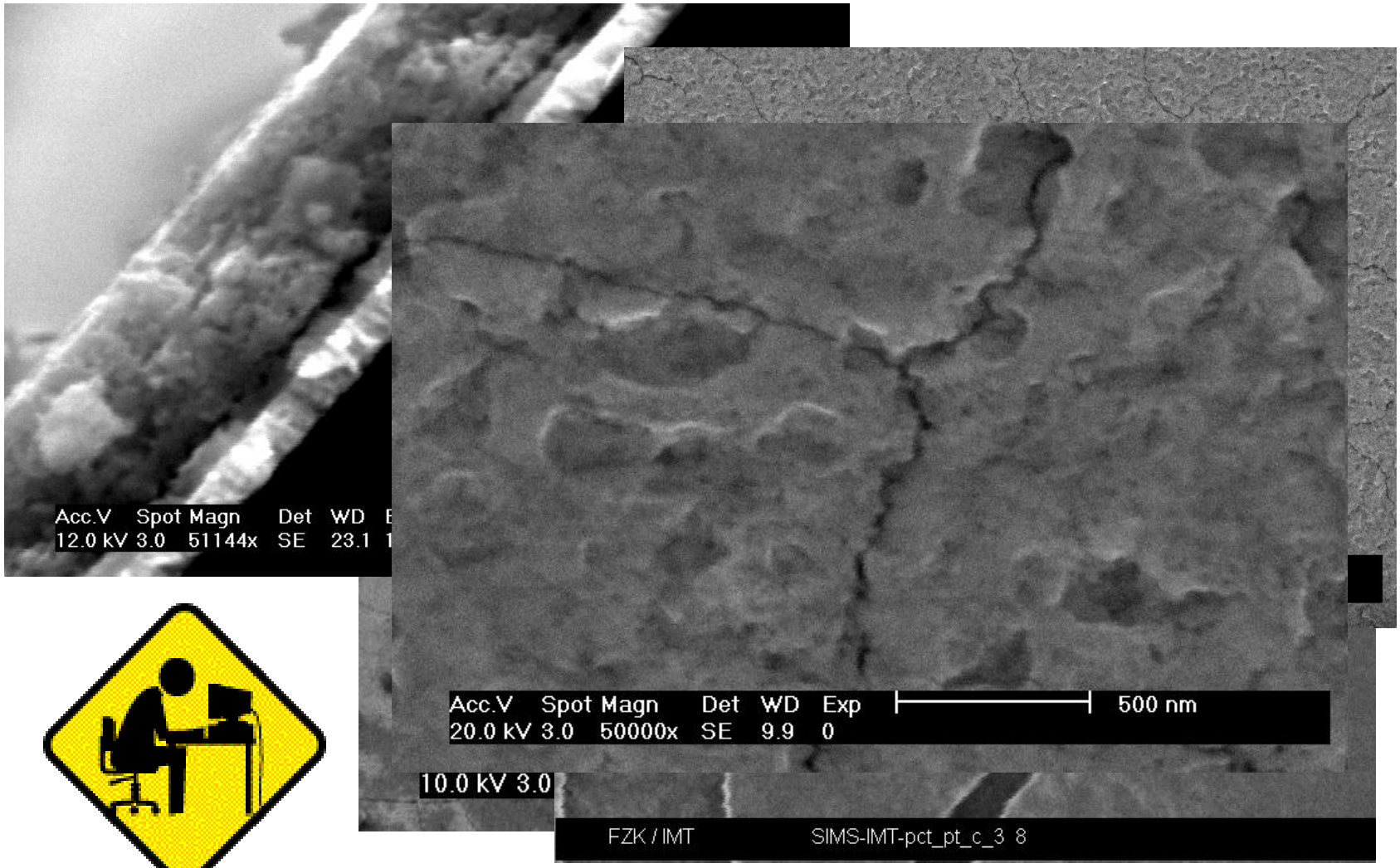

$(Pb, Sr)TiO_3$ – a "good-natured" perovskite

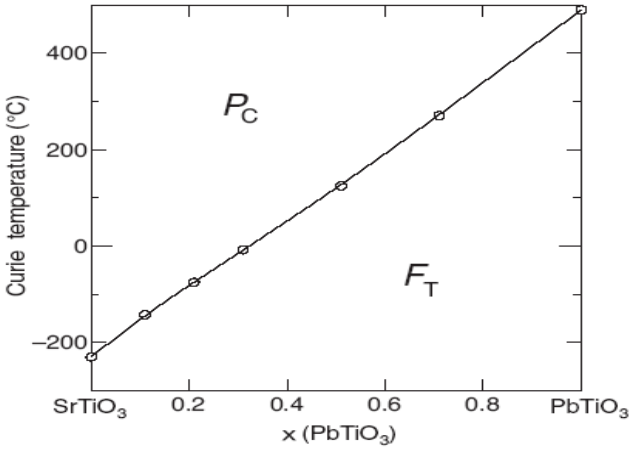

Phase diagram for $(Pb,Sr)TiO_3$

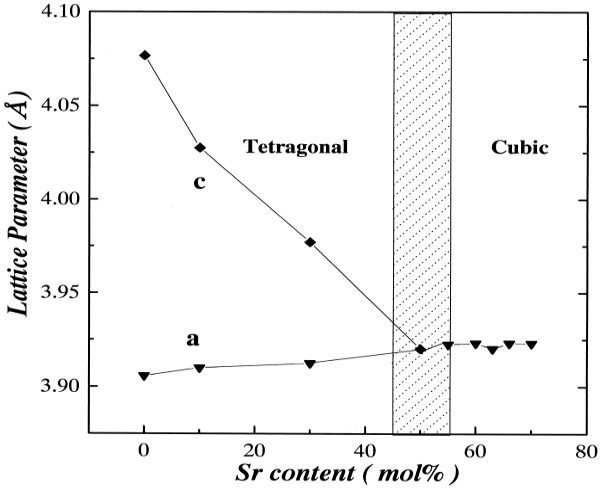

Lattice parameters for $(Pb,Sr)TiO_3$ vs. Sr content

Phase Transition from tetragonal, ferroelectric, to cubic, paraelectric, at room temperature with a Pb/Sr ratio of ~**50/50**

Only one Phase Transition is known (compared to three in $BaTiO_3$ and $(Ba,Sr)TiO_3$

Easy to realise a **crack-free** thin film via Sol-Gel

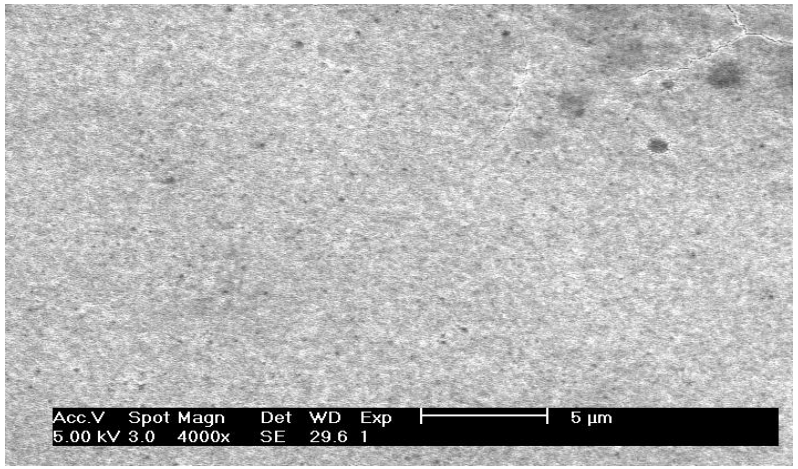

$(Pb, Sr)TiO_3$ – Sol-Gel Preparation

Lead acetate

Strontium acetate

Manganese Acetate

Titanium Butoxide

Acetic acid + 1,3 propanediol

Acetic Acid

Stirring + heating

Precursor Solution ~ 16h stirring

2-Methoxyethanol

Spin coating (30 sec @ 3000 rpm)

Bake (10 min @ 350 °C)

Annealing (15 min @ 650 °C)

PST Thin Film

XRD Analysis – The Crystallisation of PST

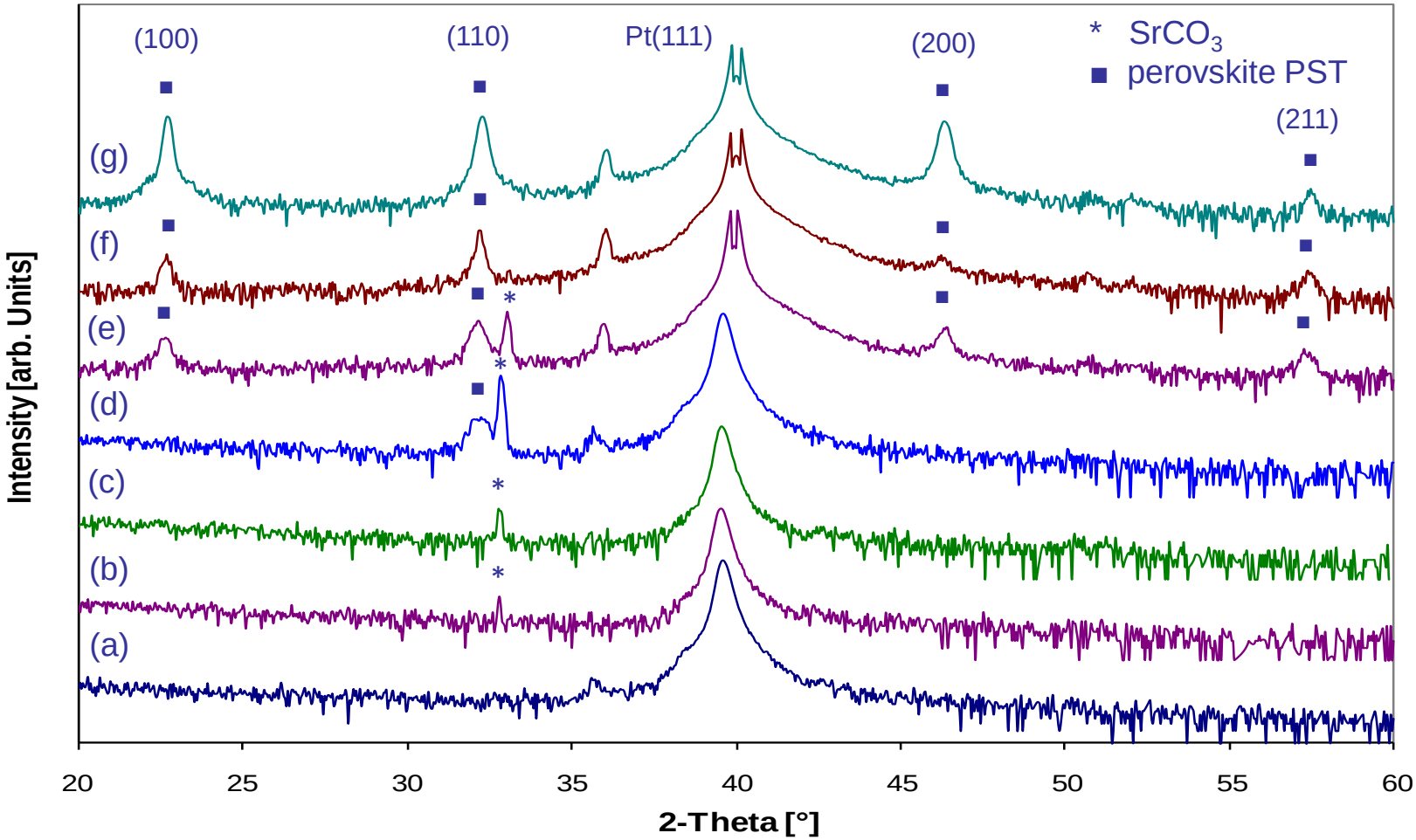

X-ray diffractograms of PST after 15 minutes at (a) 350°C, (b) 400°C, (c) 450°C, (d) 500°C, (e) 550°C, (f) 600°C and (g) 650°C.

Dielectric Properties of PST 50/50

Low frequency (10 – 300 kHz)

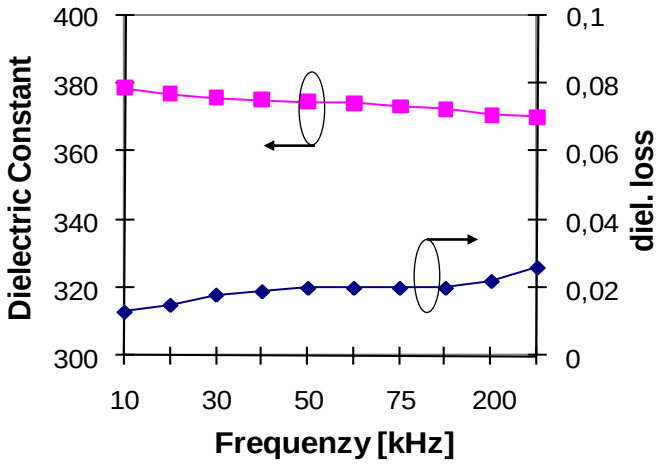

High frequency (10 – 110 MHz)

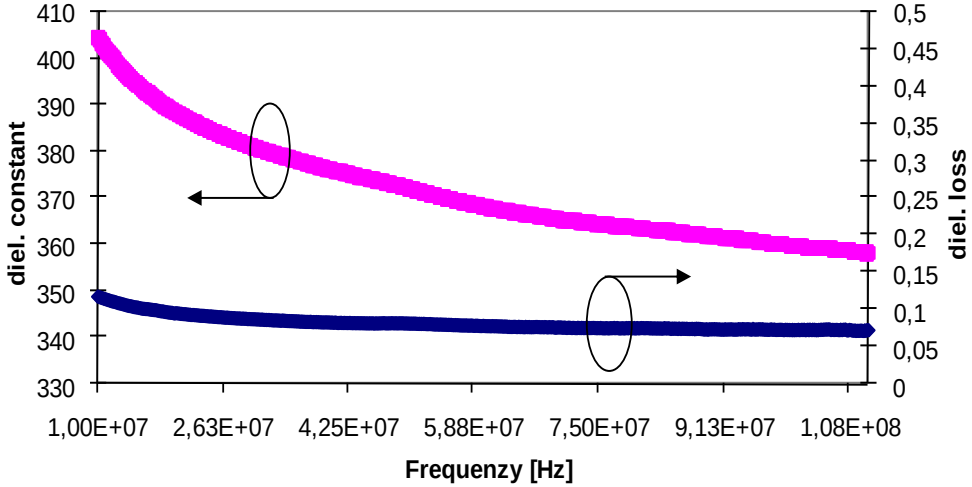

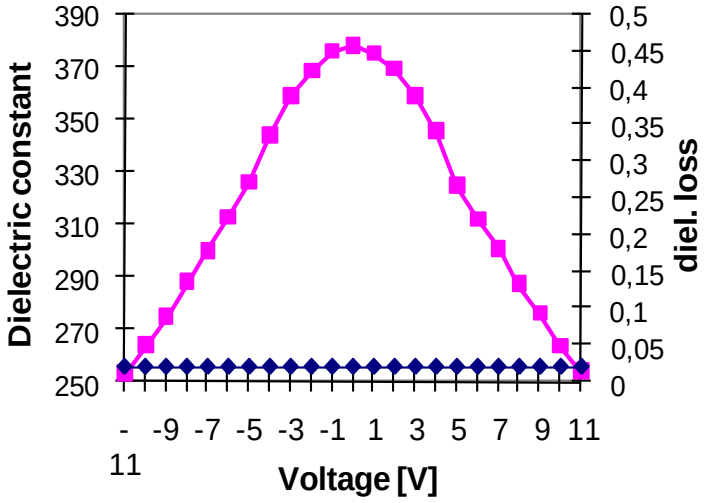

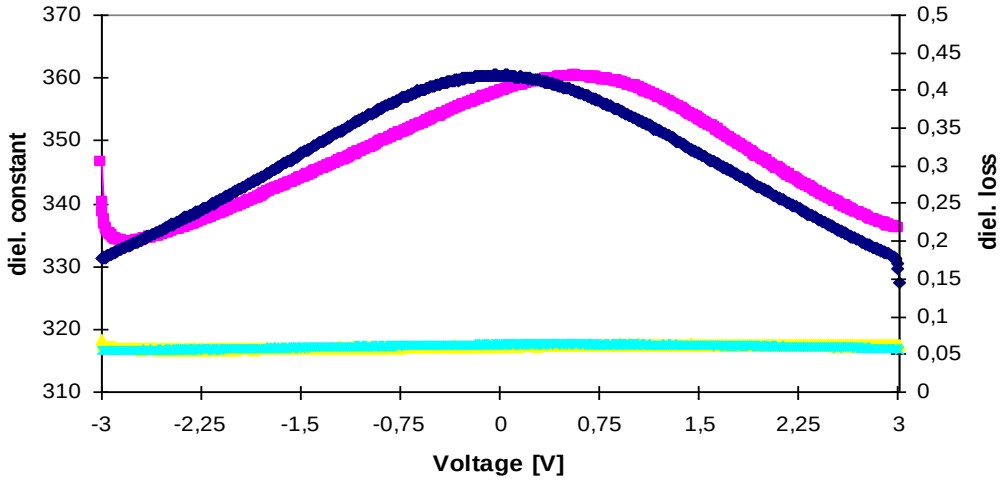

Enhanced Quality Factor with Cu Electrodes

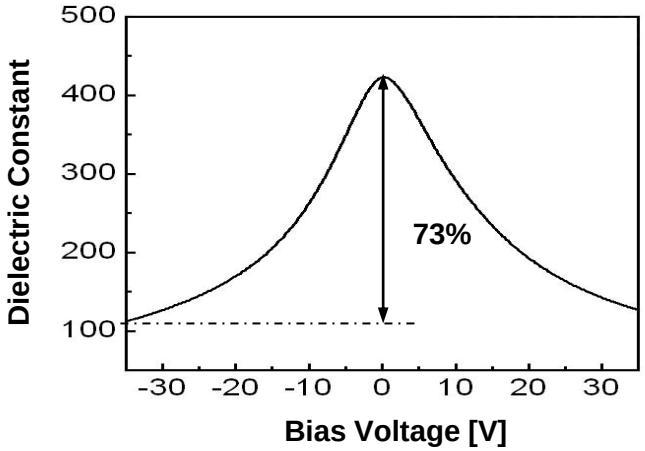

Permittivity vs. bias voltage at 1 MHz

$$\tan\delta_{device} = \frac{1}{Q_{device}} = \frac{1}{Q_{dielectric}} + \frac{1}{Q_{electrode}}$$

$$Q_{electrode} = \frac{1}{\omega R_S C}$$

Bulk Resistivity:
R_{Pt}=10.8μΩcm
R_{cu}=1.7μΩcm

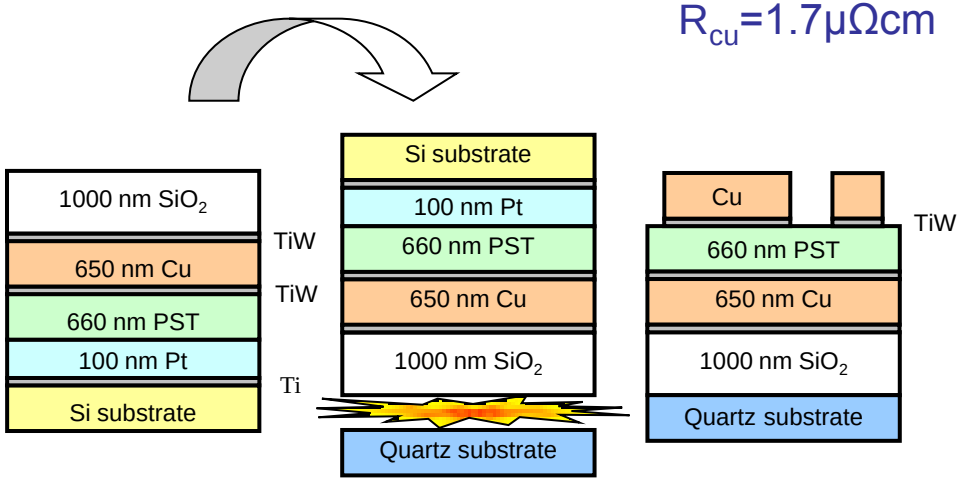

Schematic illustration of the fabrication of Cu/PST/Cu varactors by layer transfer

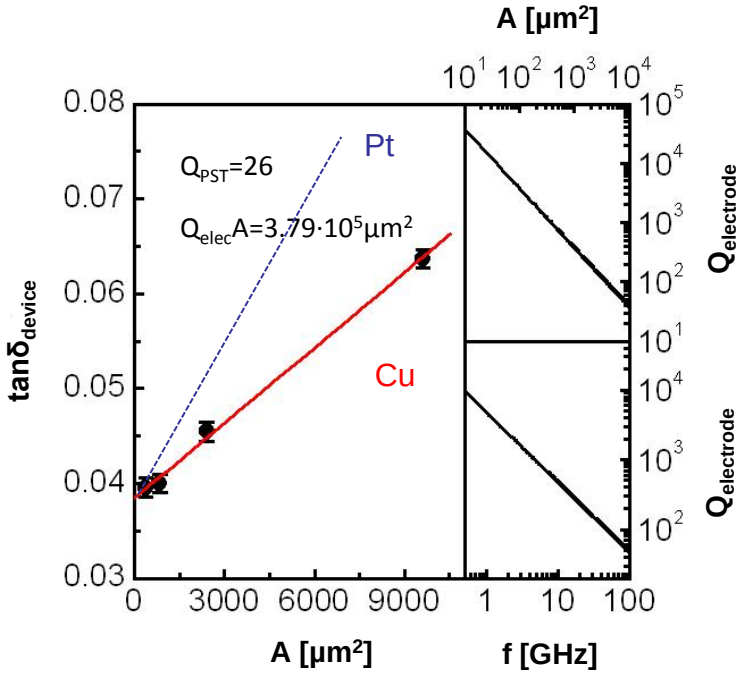

Measured dielectric loss as a function of Cu/PST/Cu capacitor area at 1GHz. The upper right and lower right graphs show the variation of the electrode quality factor as a function of capacitor size at 1GHz and frequency for a capacitor with a diameter of 10μm.

TEM Analysis of Cu/PST/Cu Varactors

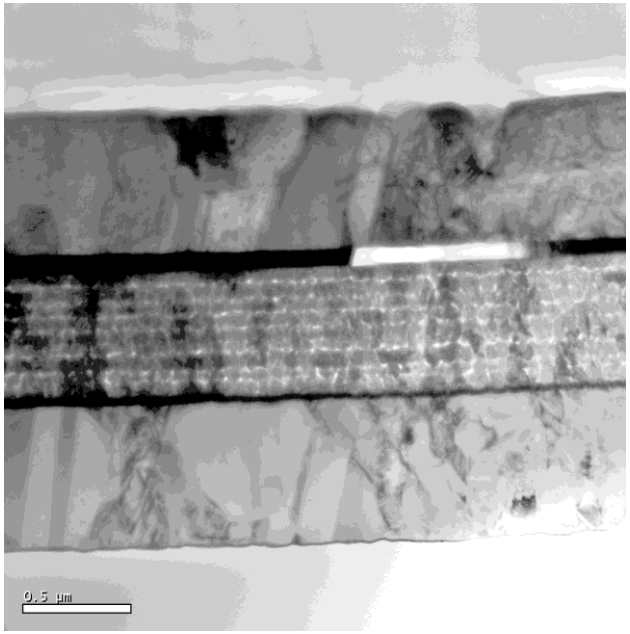

Bright-field TEM of the Cu/PST/Cu varactor

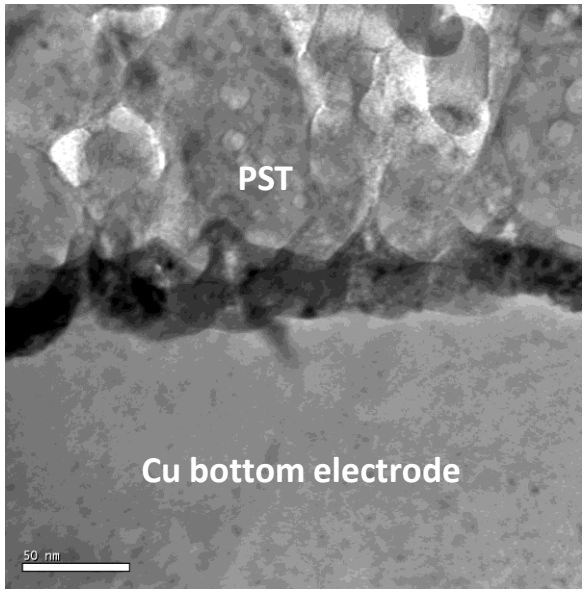

TEM image of the Cu bottom electrode/PST interface

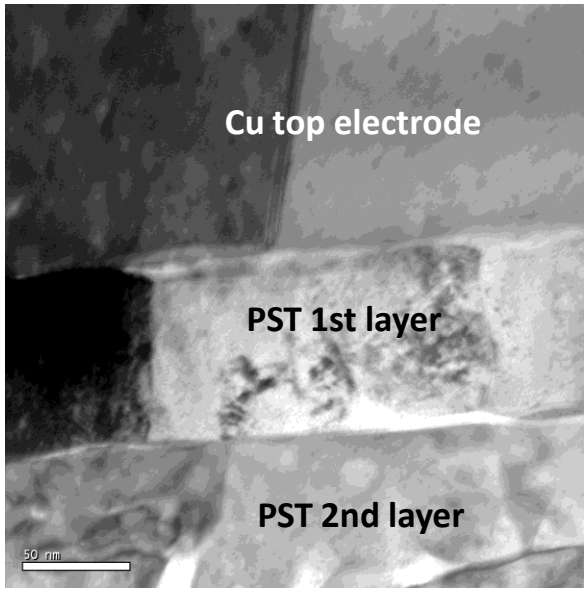

TEM image of the PST/Cu top electrode interface

- Single PST layer thickness ~ 50 nm
- Dark, rough, interlayer between PST and Cu bottom electrode (TiW layer which diffuses into the ferroelectric thin film)
- Sharp interface between Cu top electrode and 1st PST layer (good removal of the Pt/Ti seed layer)
- Sharp interface between 1st and 2nd PST layer (different layer morphology is due to dissimilarities between the films onto which these layers were spun)

B-Site Doping of PST 40/60 (Mn-doping)

Change of composition: Shift of T_C to lower temperatures.

Mn doping has an effect of the grain size of PST:

- PST pure: ~ 100 nm
- 1 mol% Mn: ~ 80 nm
- 3 mol% Mn: indistinct
- 5 mol% Mn: sponge-like

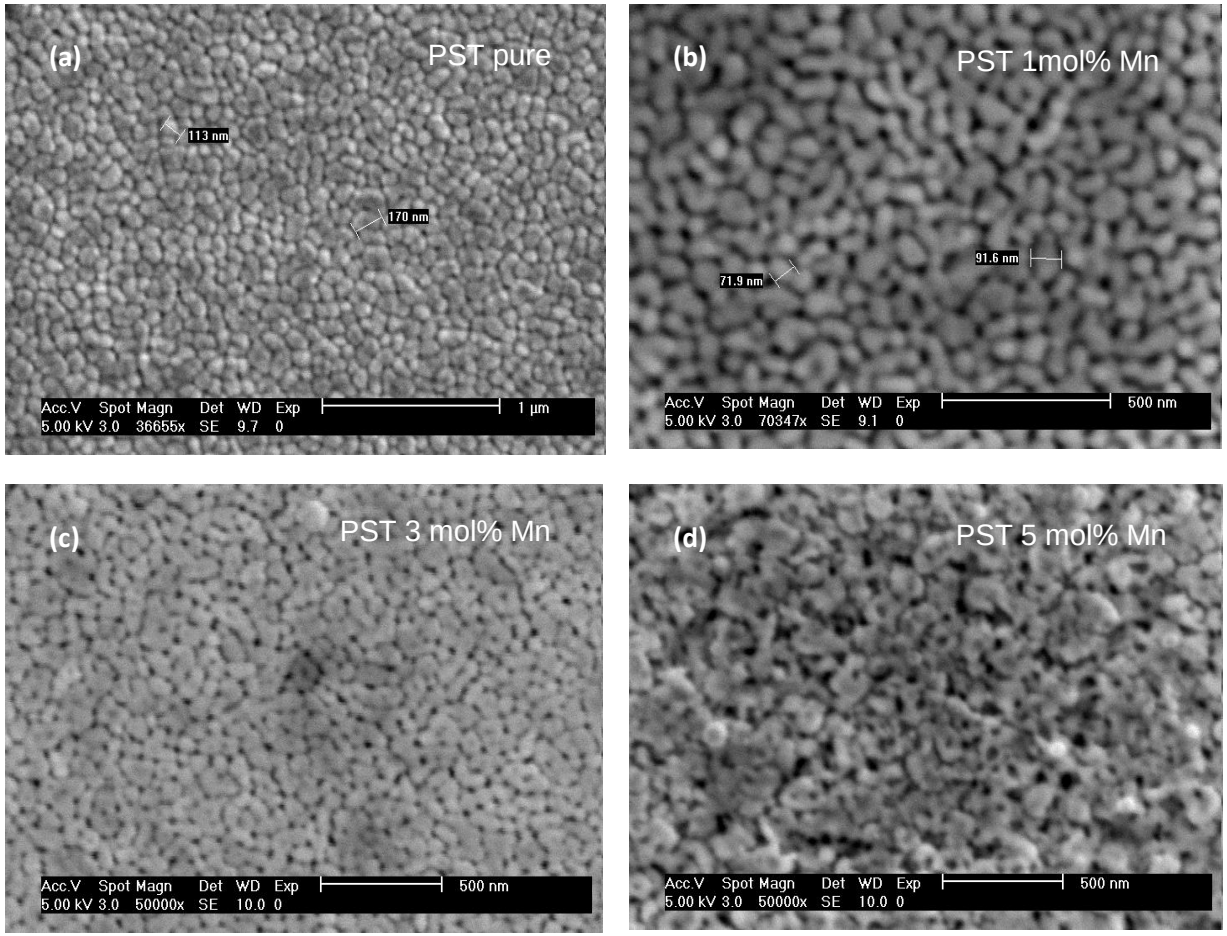

SEM images of $(Pb_{0.4},Sr_{0.6})(Ti_{!-x},Mn_x)O_3$. (a) x=0, (b) x=0.01, (c) x=0,03 and (d) x=0.05

Dielectric Properties and Roughness of Mn doped PST

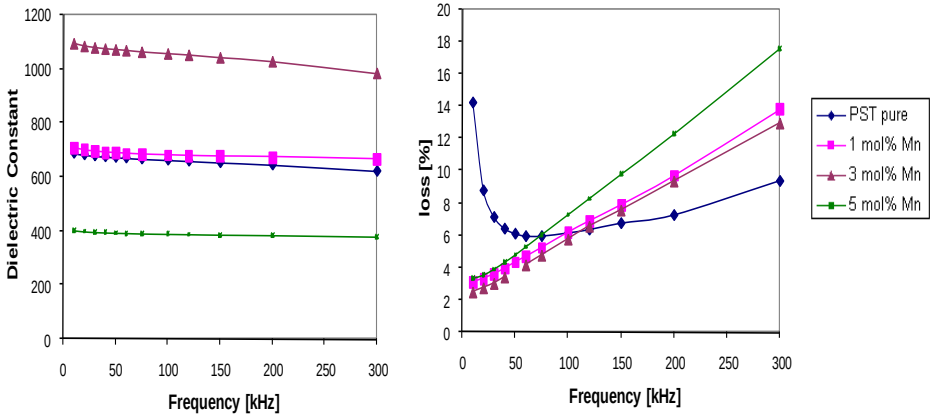

Dielectric Constant and loss vs. frequency forPST 40/60 with different Mn content

- The dielectric constant increases with increasing Mn content up to 3 mol% and decreases there after.

- The roughness/grain size is decreasing with increasing Mn content.

<u>There is no clear evidence that the film roughness/grain size is related to the dielectric behaviour in B site doped PST.</u>

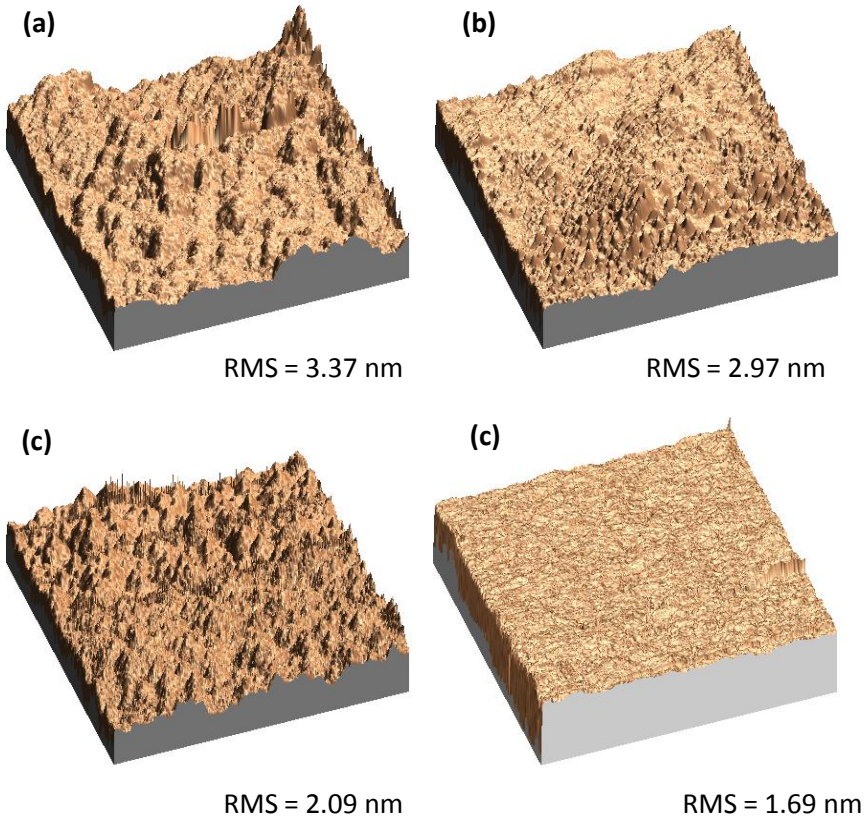

*AFM images of $(Pb_{0.4},Sr_{0.6})(Ti_{!-x},Mn_x)O_3$. (a) x=0, (b) x=0.01, (c) x=0,03 and (d) x=0.05. Scan size: 2*2 µm*

The Reason for the Increase of the Dielectric Constant for x < 0.02

1. Oxygen vacancies are generated by heat treatment

$$2Ti^{4+} \rightarrow 2Ti^{3+} + V_O^{\bullet\bullet}$$

2. Mn is a multivalence ion – it can appear as Mn^{2+}, Mn^{3+} and Mn^{4+}

$$\frac{1}{2}O_2 + Mn^{2+} + V_O^{\bullet\bullet} \rightarrow Mn^{4+} + O_O^X \qquad \frac{1}{4}O_2 + Mn^{2+} + \frac{1}{2}V_O^{\bullet\bullet} \rightarrow Mn^{3+} + \frac{1}{2}O_O^X$$

$$\Rightarrow \begin{cases} 2Ti^{4+} + Mn^{2+} + \frac{1}{2}O_2 \leftrightarrow 2Ti^{3+} + Mn^{4+} + O_O^X \\ 2Ti^{4+} + Mn^{2+} + \frac{1}{4}O_2 \leftrightarrow 2Ti^{3+} + Mn^{3+} + \frac{1}{2}O_O^X \end{cases}$$

Mn^{2+} doping consumes oxygen vacancies in PST to get incorporated as Mn^{3+}/Mn^{4+} at the Ti^{4+} site

Mn doping induces a negative charge and thus balances the positive of the oxygen vacancies. Then with the charge being compensated, **the lattice distortion ratio in the system decreases**, viz. the lattice structure of $Pb_{0.4}Sr_{0.6}Mn_xTi_{1-x}0_3$ becomes more perfect (cubic). According to the thermodynamic theory, **the phase formation ability of the crystal is therefore increased** with increasing Mn content up to 0.02. At the same time, **more polarisation path may be provided** when the lattice structure becomes more perfect. **So the dielectric constant of the film is correspondingly increased.**

The Behaviour of Dielectric Properties in Mn doped PST

$x < 0.02$: Mn^{2+} doping consumes oxygen vacancies, thus providing a larger polarisation path. **The dielectric constant increases**

$x \sim 0.02$: The positive charge of the oxygen vacancies is totally balanced by the negative of Mn^{2+}, Mn^{3+}, or Mn^{4+}. **The system is saturated.**

$x > 0.02$: **Electron hopping between Mn^{2+}, Mn^{3+} and Mn^{4+} begins**. The hopping conduction due to the hopping of the charge carriers between Mn sites begins to occur in 2 mol% Mn doped PST, and then becomes distinct in 5 mol% doped films. **This lowers in the end the dielectric constant and increases the loss in PST thin films**

The Tunability in Mn doped PST

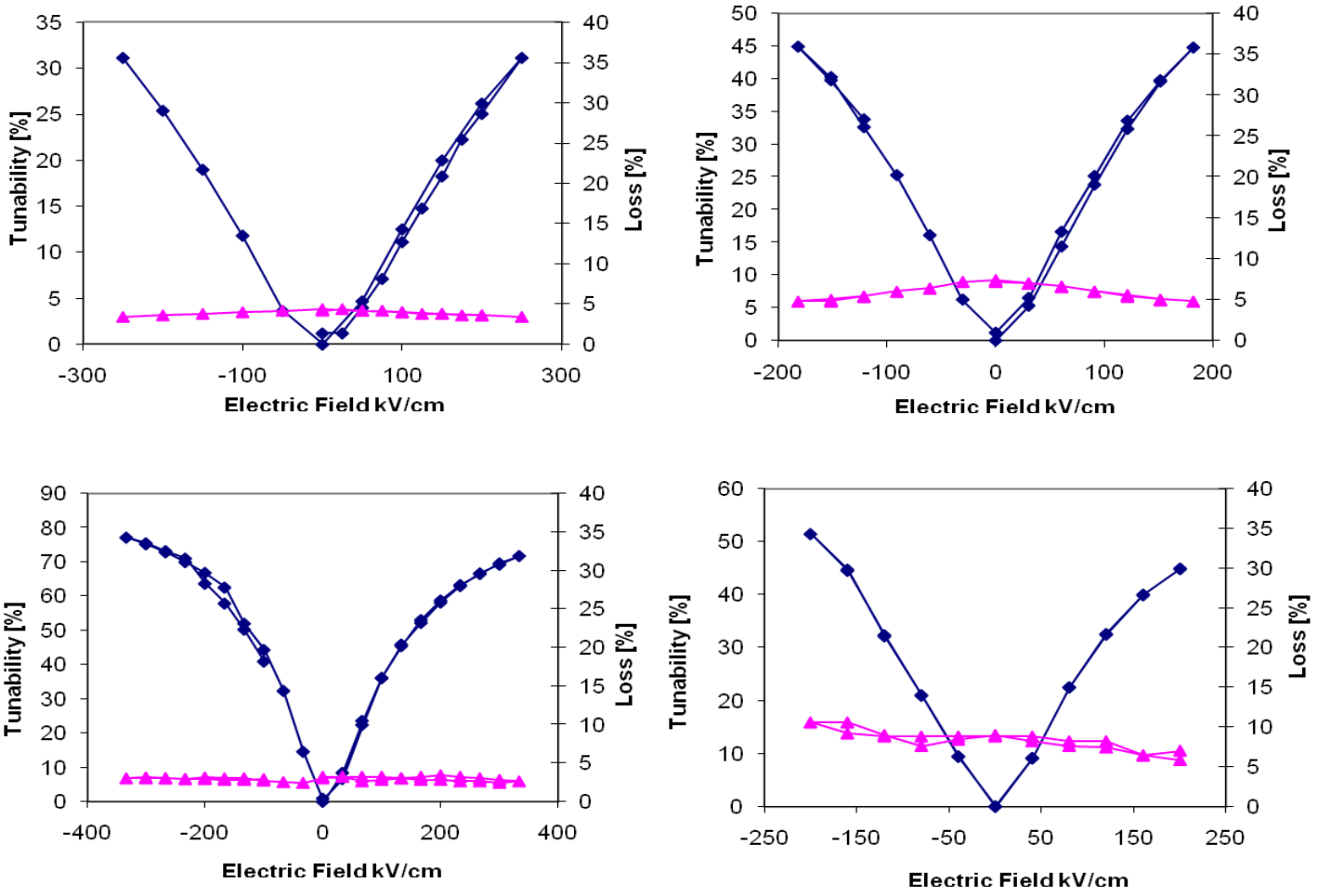

Tuanability and loss vs electric field at 150 kHz of $(Pb_{0.4},Sr_{0.6})(Ti_{1-x},Mn_x)O_3$. (a) x=0, (b) x=0.01, (c) x=0,03 and (d) x=0.05

Comparison between Measured and Theoretical Tunability

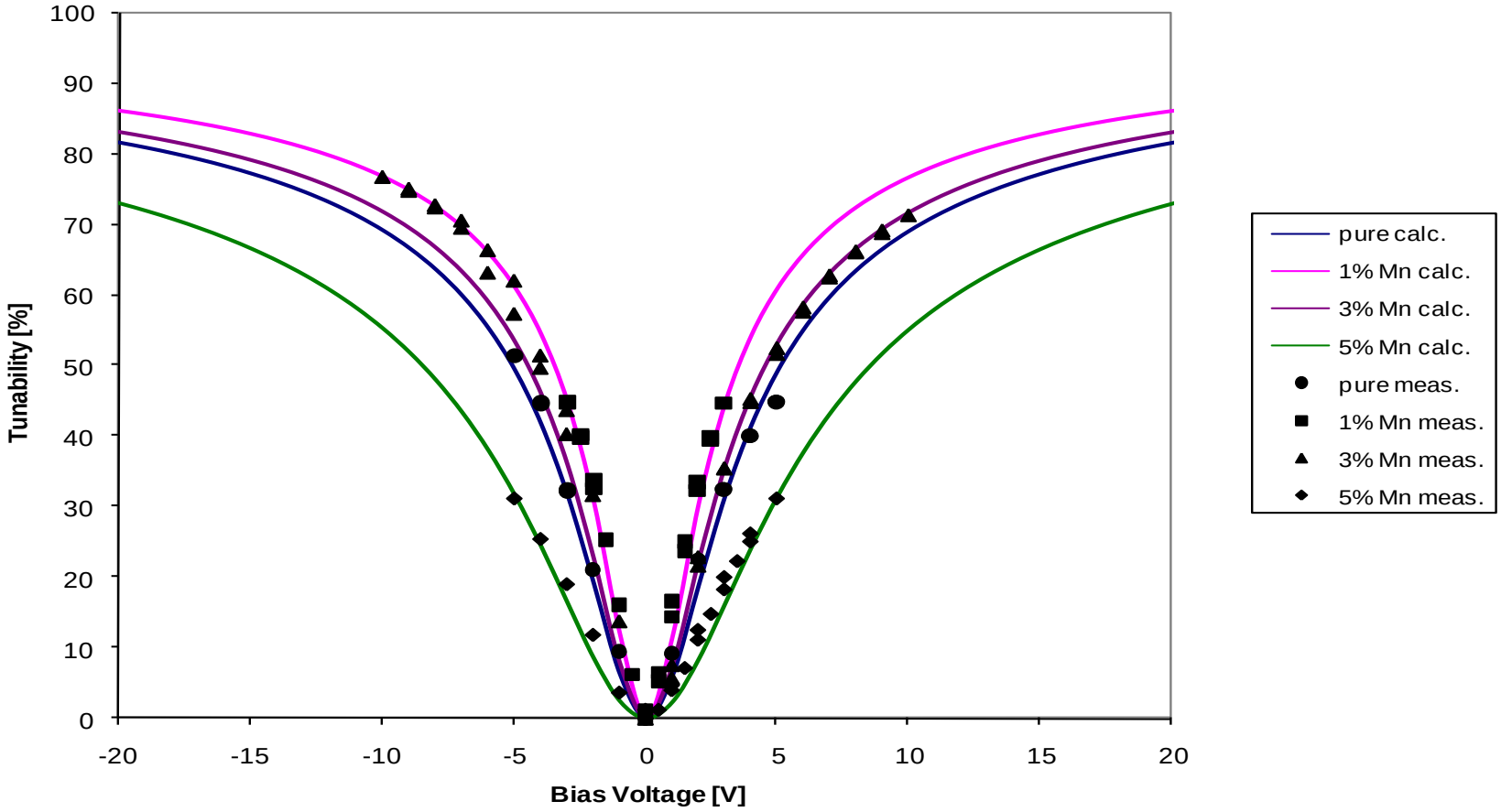

Comparison o fthe measured and calculated tunability of $(Pb_{0.4},Sr_{0.6})(Ti_{!-x},Mn_x)O_3$

The Change of T_C with Mn doping

T_C increases with increasing Mn content

Mn [mol%]	T_C [°C]
0	13
1	17
3	22
5	26

T_C for 5 mol% Mn above room temperature → ferroelectric

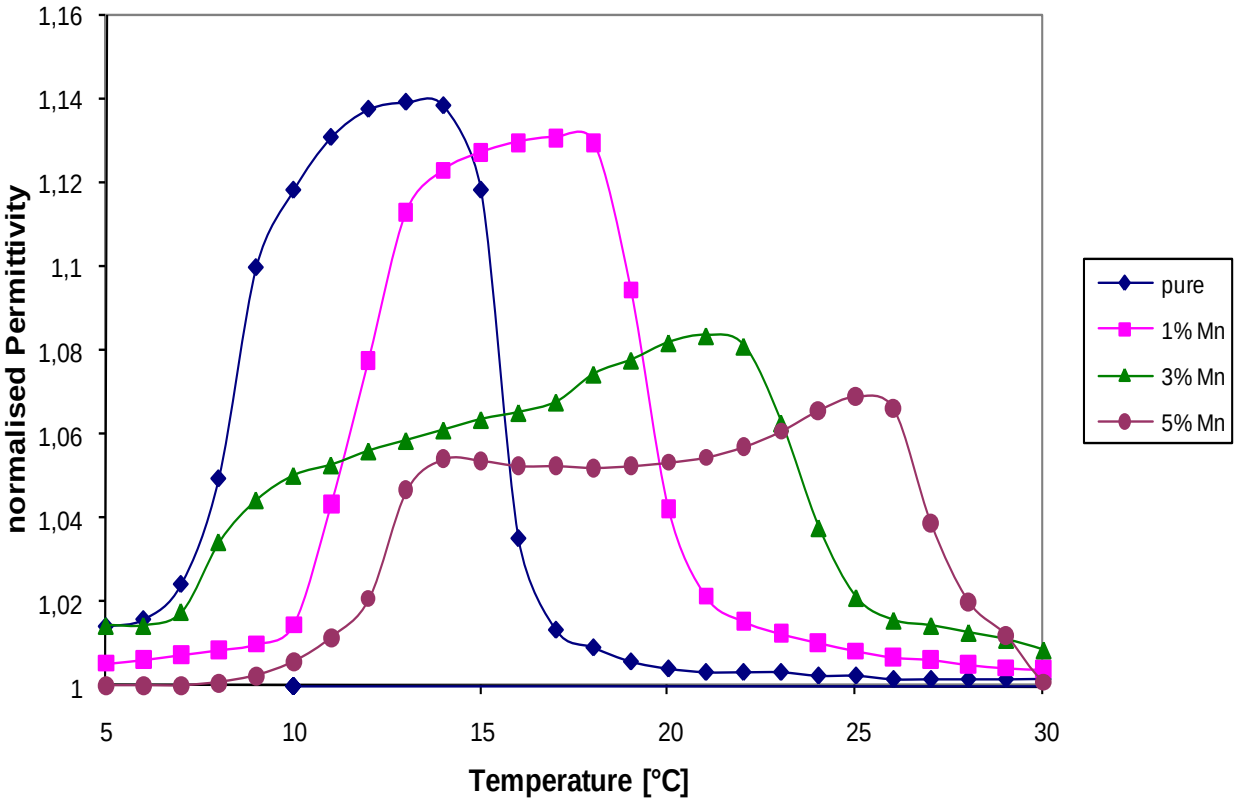

Normalised Permittivities vs temperature of $Pb_{0.4}Sr_{0.6}Mn_xTi_{1-x}0_3$

The origin of the the broadening of the peak for 3 mol% and the double peak for 5 mol% Mn is unclear. This could be an indication of **an increasing relaxor behavior of PST** with increasing Mn content. Unfortunately the home-made measuring equipment was not sensitive enough to measure the frequency dispersion of the dielectric maximum, which would be a clear indication for relaxor ferroelectrics.

Enhanced Ferroelectricity with Mn doping

The behaviour of the Hysteresis proofs the enhancement of the ferroelectricity in PST with increasing Mn doping.

The slim loop is a further indication of relaxor-like behaviour *):

Normal ferroelectric

relaxor

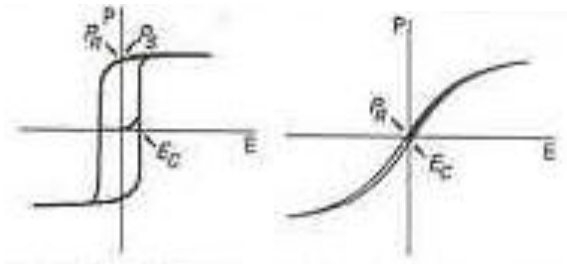

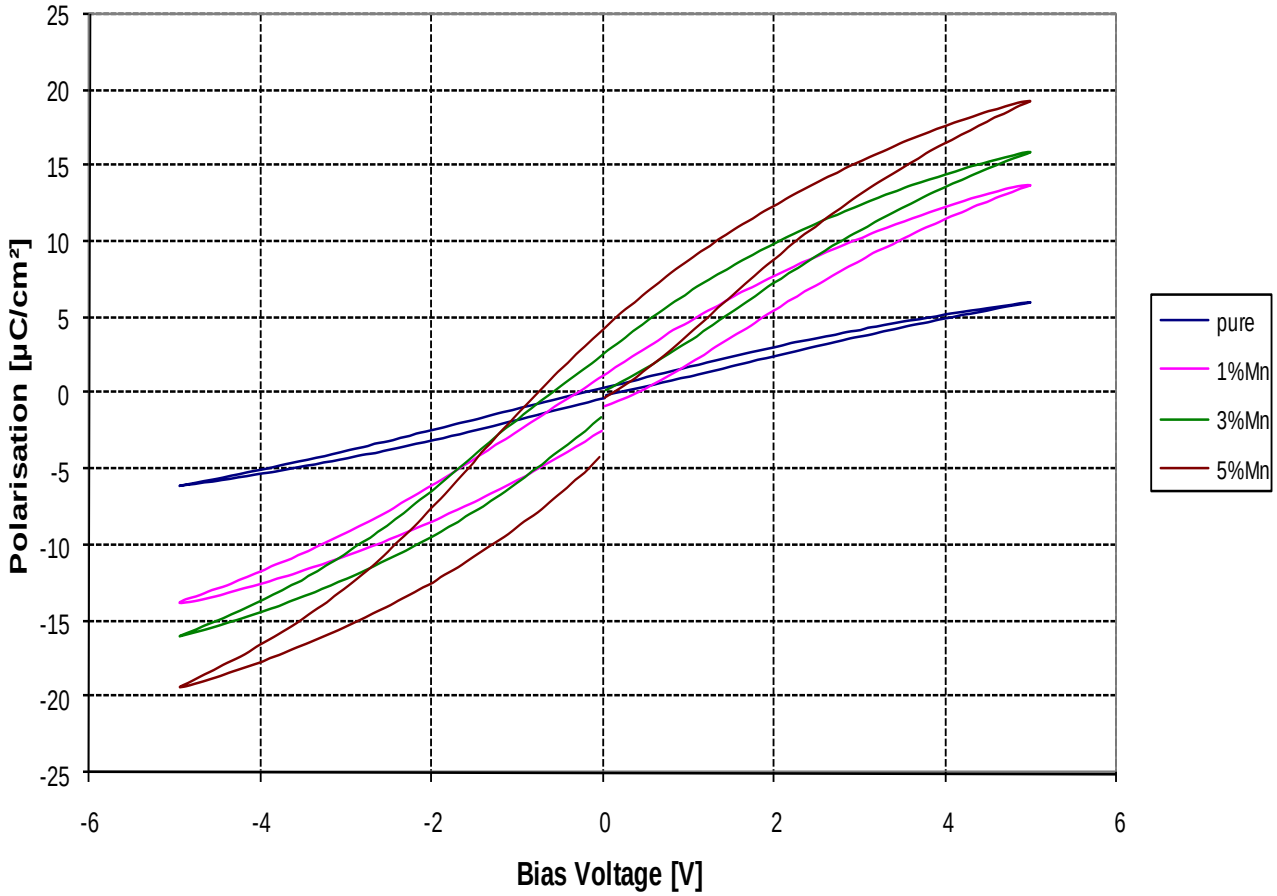

Hysteresis loops of $Pb_{0.4}Sr_{0.6}Mn_xTi_{1-x}0_3$.

The film is paraelectric with x=0 and the ferroelectricity improves with x.

*) Temperature at which the dielectric constant is maximum shifts to higher temperature with increase in freqeuncy

Summary

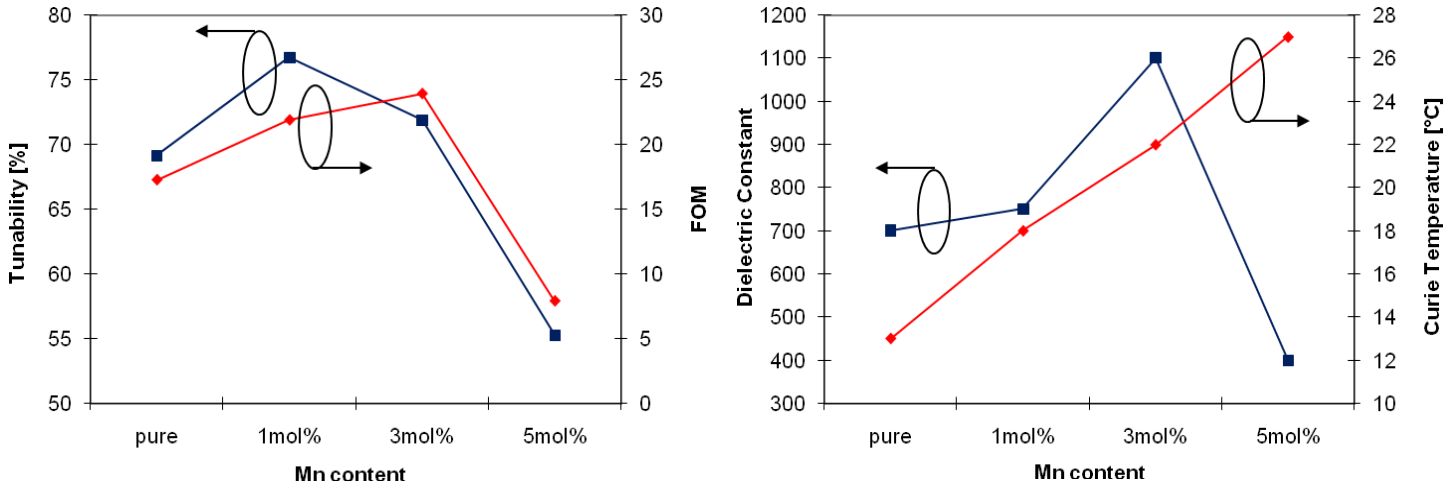

Tunability and figure of merit at 10V and dielectric constant and Curie temperature at zero biasof PST 40/60 with different Mn content

Improved Performance due to Mn B-site Doping

- Mn^{2+} doping consumes oxygen vacancies (a common defect in ferroelectric thin films)
- For Mn > 2-3 mol% hopping of charge carriers between Mn sites occurs
- This degrades the film and its properties

Enhanced Tunability with Mn Doping

Max Tunability ~80% with 2% loss → K-Factor 40

Phase Transition shifts to higher Temperatures due to an enhancement of Ferroelectricity

Indication of relaxor-like behaviour in Mn-doped PST

$Pb_{0.4}Sr_{0.6}Mn_{0.03}Ti_{0.97}O_3$ directly on SiO_2

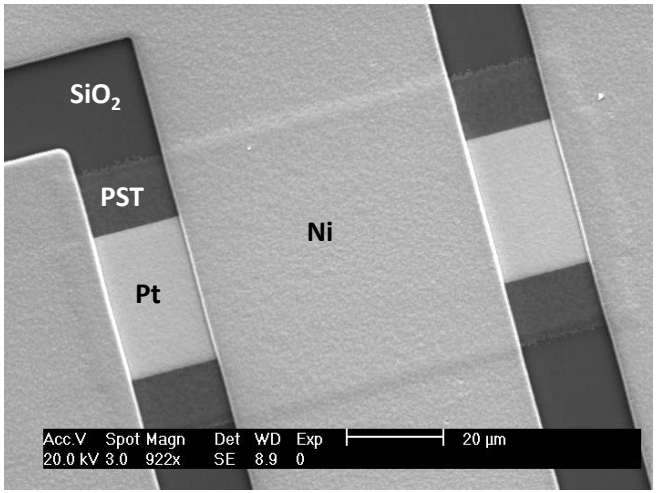

PST on SiO_2 and patterned Pt bottom electrode

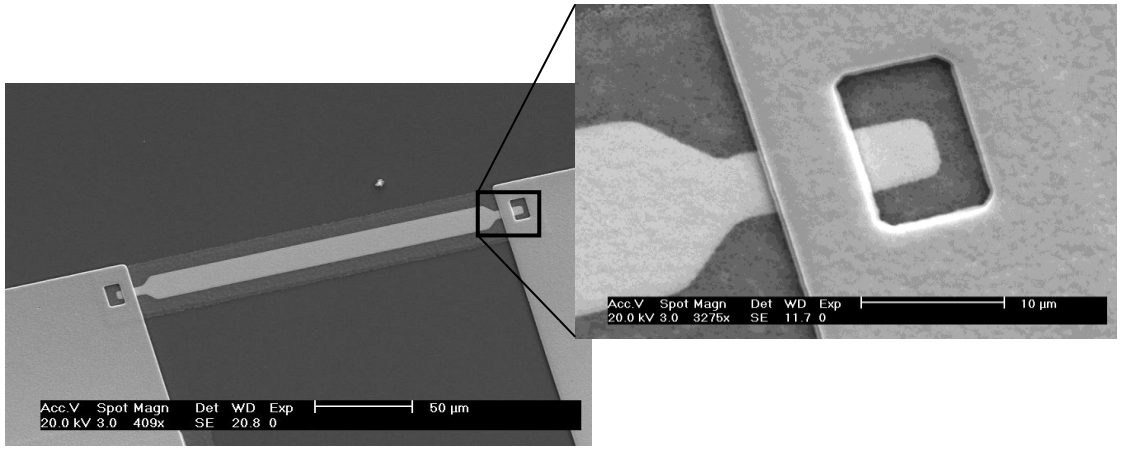

A slotted PST varactor to minimise the variation of the capacitor ares due to mask alignment errors.

- Ferroelectric thin films like PZT and BST often need a metallic-like layer on top of the substrate to promote a crack-free (highly orientated) growth.
- The most common metallic layer is Pt due to its high chemical resistance, relative good lattice match to the ferroelectric film, and its stability to the high temperatures required for the growth of ferroelectric thin films.
- Sometimes it is beneficial from the technological site of view to have the ability to work with a patterned bottom electrode rather than a continuous one.
- **PST can crystallise crack-free directly on SiO_2.**

The growth of PST on SiO_2

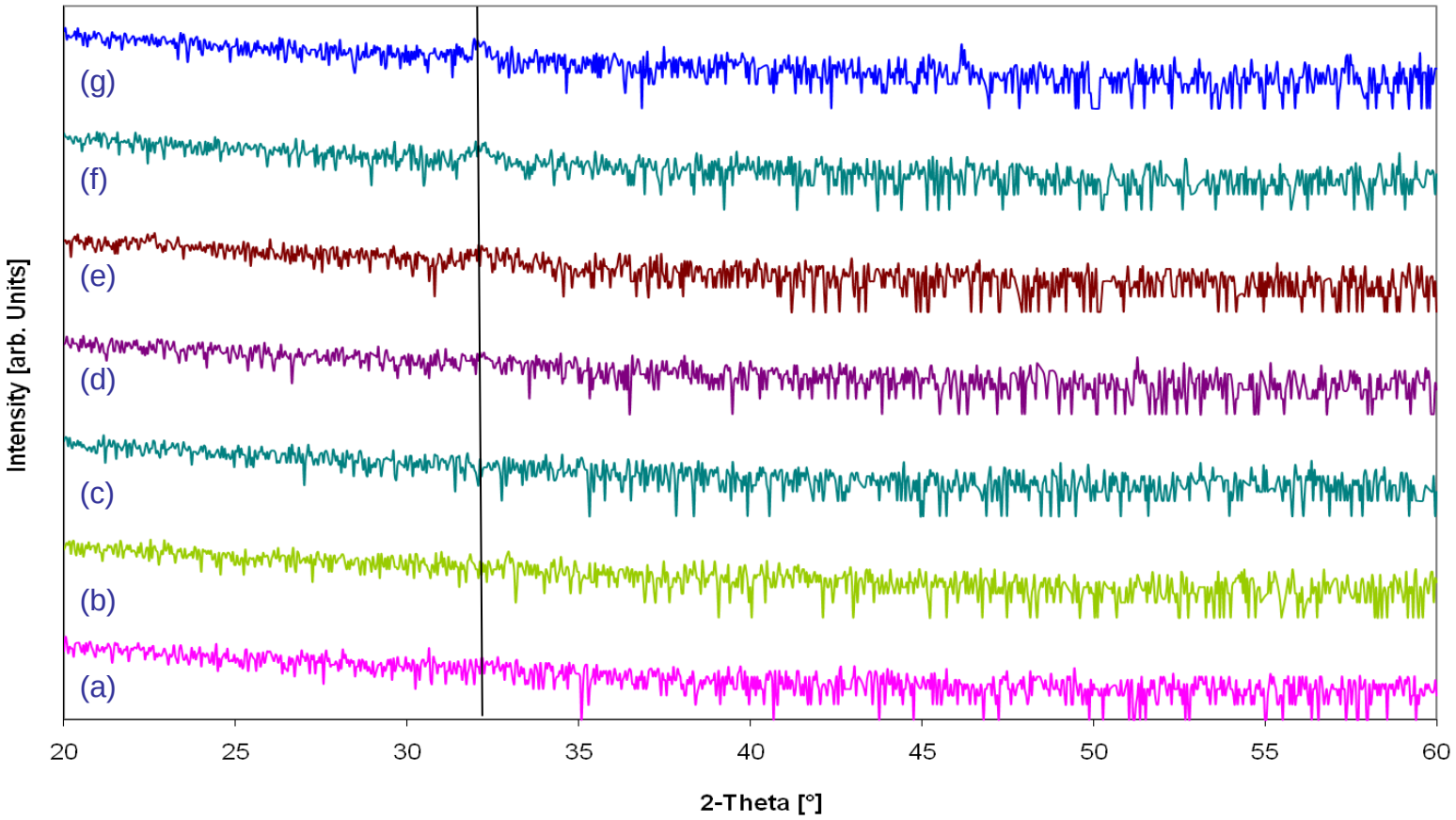

X-ray diffractograms of one layer of PST deposited directly onto SiO_2/Si and annealed for 15 minutes at (a) 350°C, (b) 400°C, (c) 450°C, (d) 500°C, (e) 550°C, (f) 600°C and (g) 650°C.

Beginning of crystallisation at 550°C. ~50°C more than on Pt/Ti

The growth of PST on SiO_2 – part II

• The roughness is increasing with annealing temperature from 0.686 to 7.905 nm for 550 and 650 °C respectively, indicating an increase in the crystallinity.

• The little pools have a depth of approximately 2 nm and their number is increasing with annealing temperature while their size is clearly decreasing.

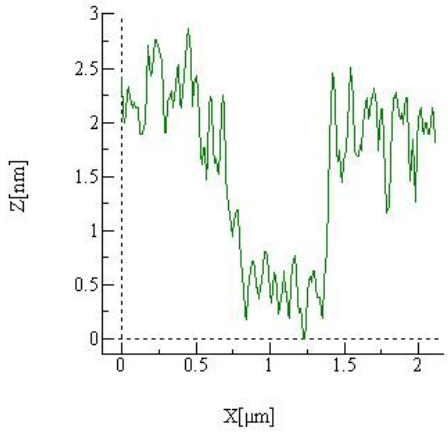

The PST thin film can be regarded to be **fully crystallised** after an annealing bake of 650°C.

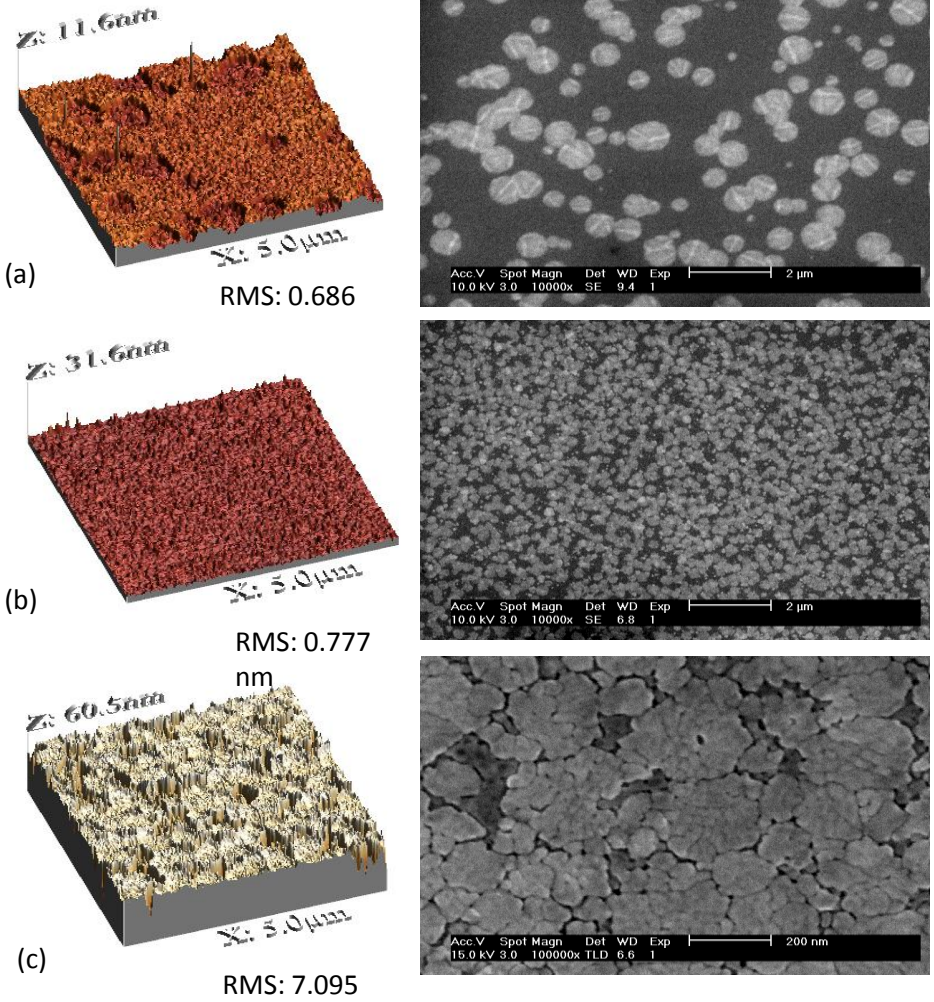

AFM- and SEM imagines of PST on SiO_2/Si annealed at (a) 550°C, (b) 600°C, and (c) 650°C

Atomistic Model of the Si (100) surface

- On the **unreconstructed silicon** surface the atoms form a square array.

- Owing to a lack of upper bonding partners, each atom has two singly occupied dangling bonds pointing out of the surface.

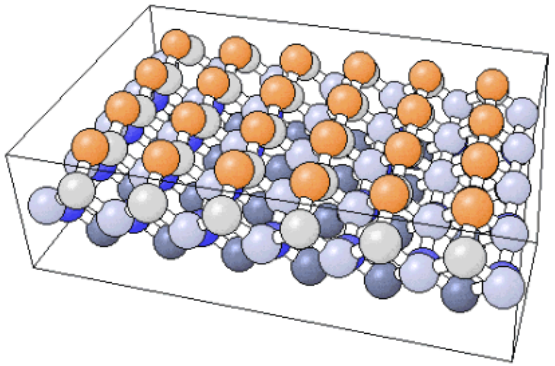

The unreconstructed Si (100) surface

- Pairs of silicon atoms dimerise, using up **one dangling bond per atom** to form a dimer bond. This is called the **"dimer row"** reconstruction (a).

- A second rearrangement leads to the **"buckled row"** reconstruction (b), in which one atom of each dimer lifts up and the other shifts down, resulting in a buckled dimer.

- This buckling causes both electrons to localise in the upper silicon atom of a dimer, whereas the other silicon atom with the empty dangling bond prefers a more planar arrangement.

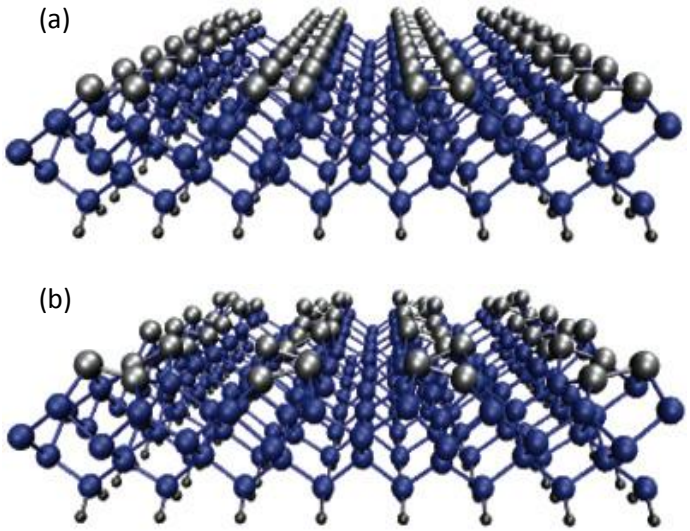

The top surface of silicon; (a), the "dimer row" reconstruction, and (b), the "buckled row" reconstruction

.

The interface between Si and $SrTiO_3$

• Even at room temperature, the buckling pattern is dynamic, with the dimers executing a kind of **"rocking" motion** or oscillation around the idealized structure. As a result the surface dimers are **chemically very reactive** and can serve as receptors for many types of atoms or even molecules.

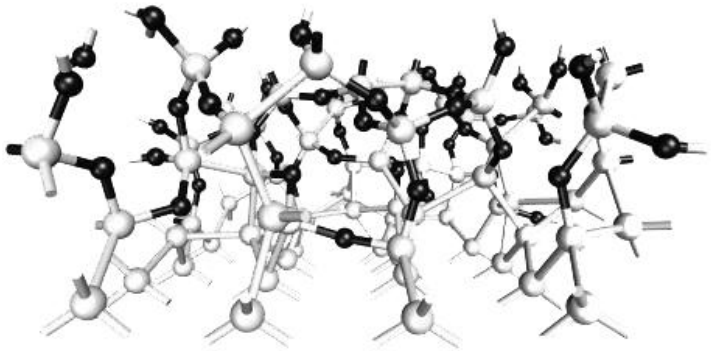

The Si-SiO_2 interface. Black atoms are Oxygen

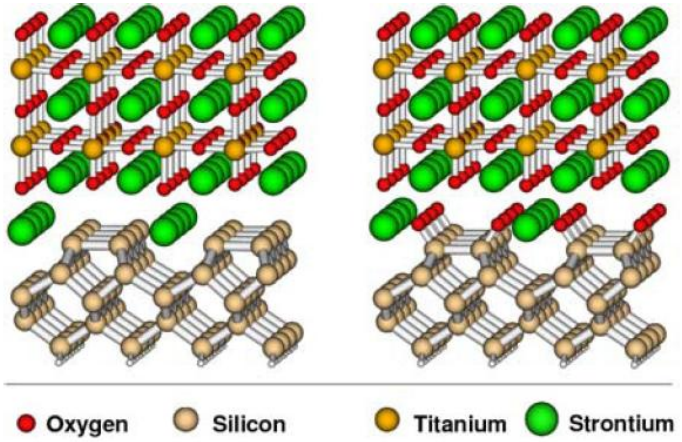

The two relevant interface structures between silicon and $SrTiO_3$

• Among them <u>oxygen</u> and **<u>strontium</u>**.

• At one half monolayer, the Sr ad-atoms occupy all favorable positions in the center of four dimers and all dangling bonds are saturated.

• The electronically saturated Si-Sr stack acts as an interfacial layer which provides a **covalent bonding environment towards the silicon substrate** and an **ionic template compatible with that of $SrTiO_3$**.

•The perovskite $SrTiO_3$, being an ionic crystal, can grow on this template and forms a second interfacial layer to PST

Auger Spectroscopy of PST- part I
1 – 21 (PST layer)

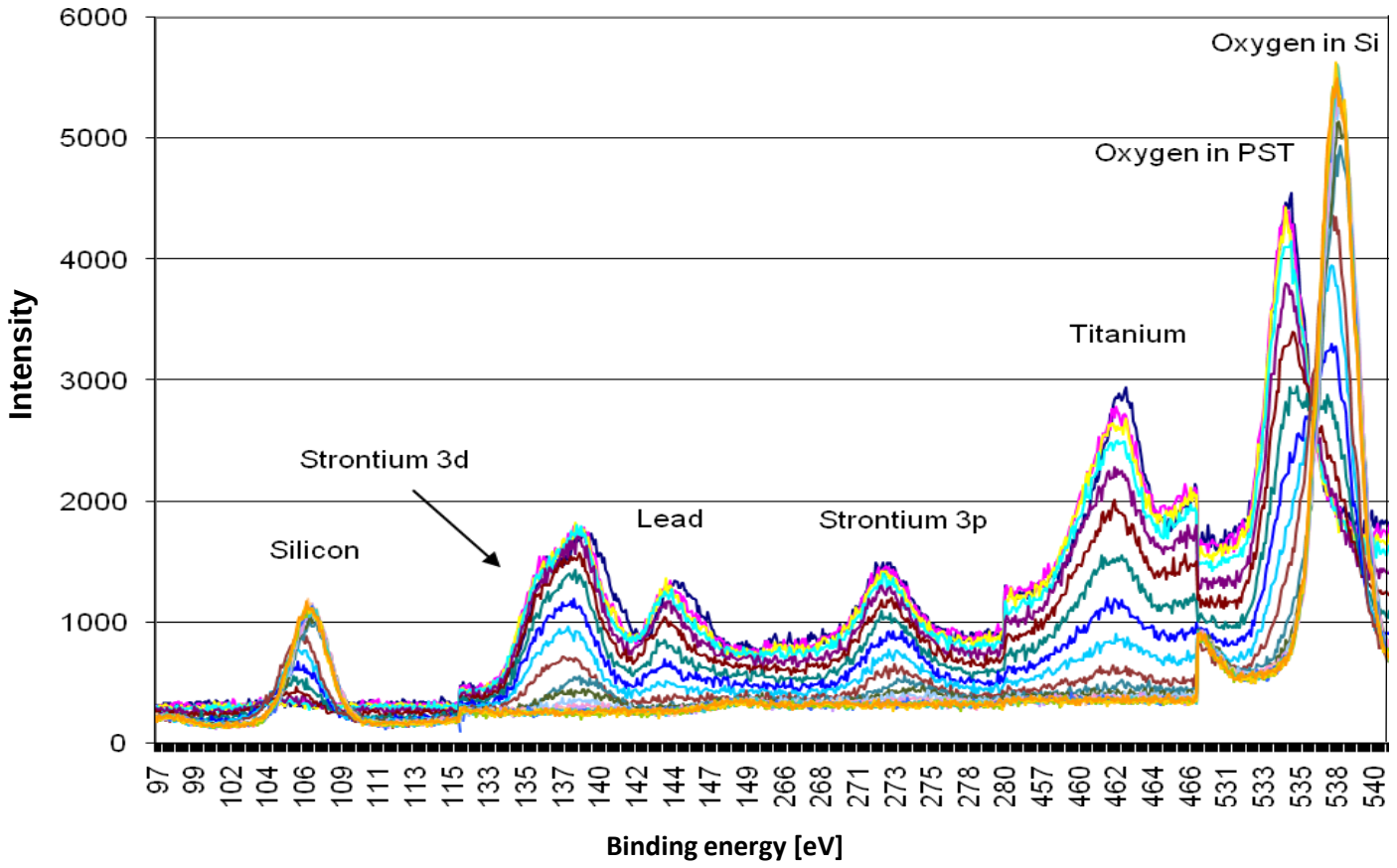

Auger spectra of one layer PST and its interface to the Si/SiO2 substrate

Etching time 100 sec per step, ion current 2kV at 0.75µA

Auger Spectroscopy of PST - part II
21 – 40 (SiO_2 layer) and 41 – 60 (getting to the Si-substrate)

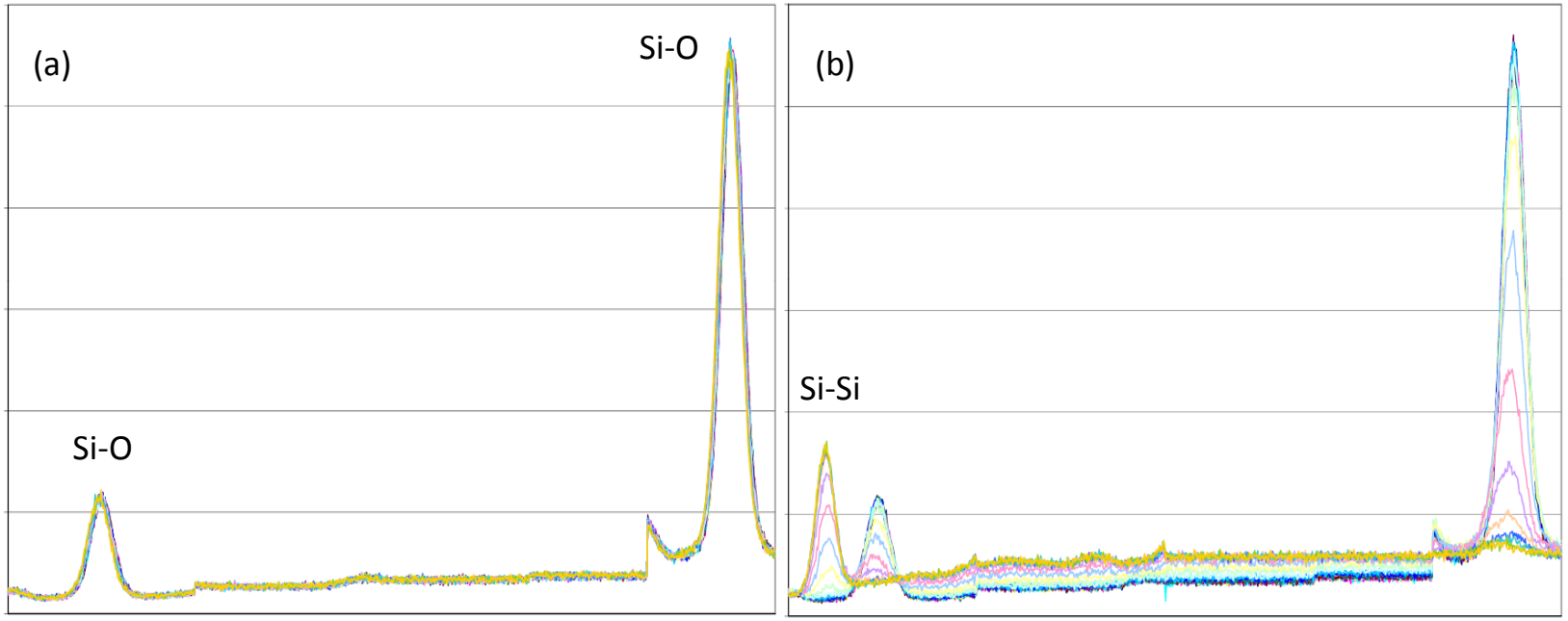

Auger spectra of the SiO2 layer (a) and the interface to the Si main substrate (b).

More than 40 etch steps were necessary to reach the Si substrate

Depth profile of 1 Layer PST on SiO_2

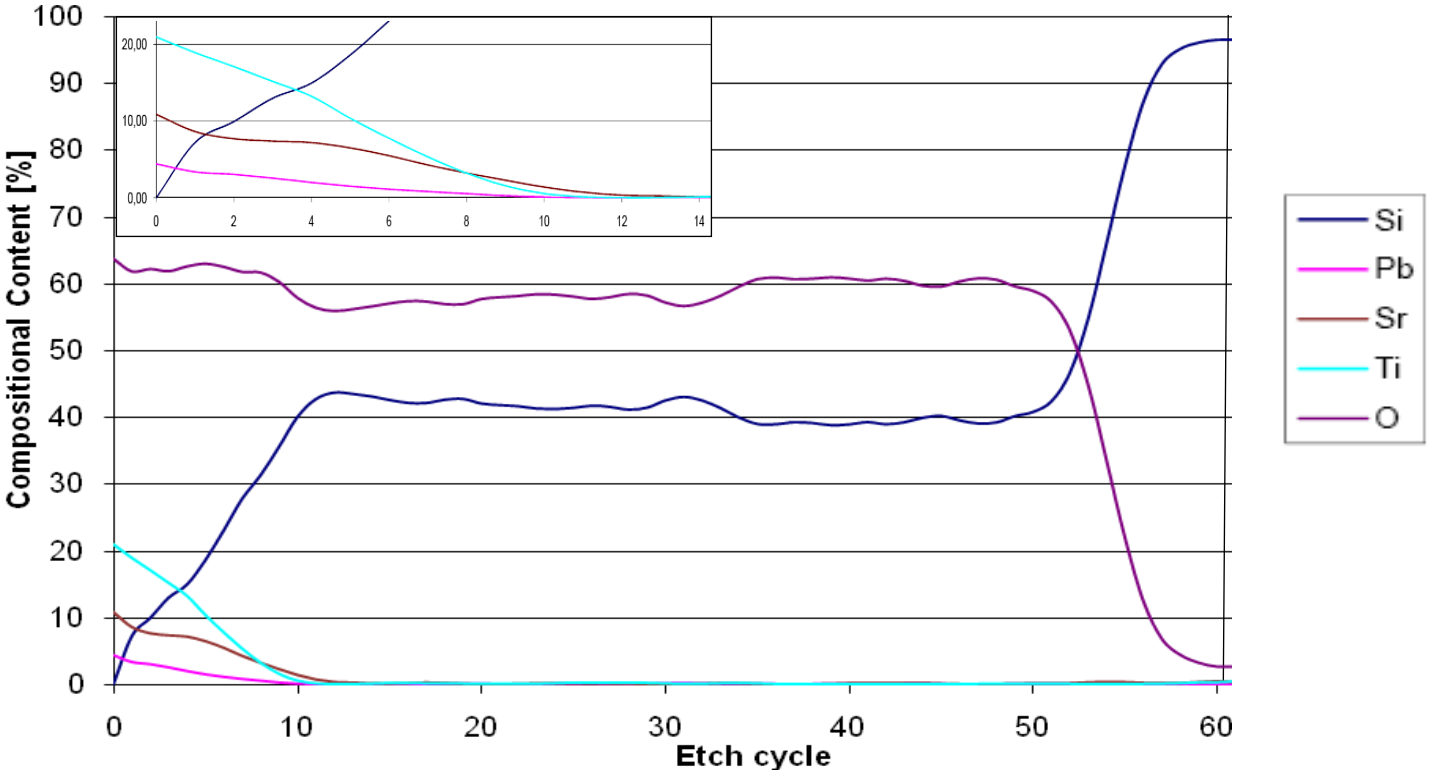

Depth profile of one layer PST on SiO_2/Si. The interface regions are clearly visible.

No Pb diffusion into the SiO_2. Sr-Ti diffusion is deeper

The broad SiO_2 area is the dominant feature in this graph and the SiO_2-Si interface is clearly distinguishable

Comparison: Depth profile of 1 Layer PZT on SiO_2

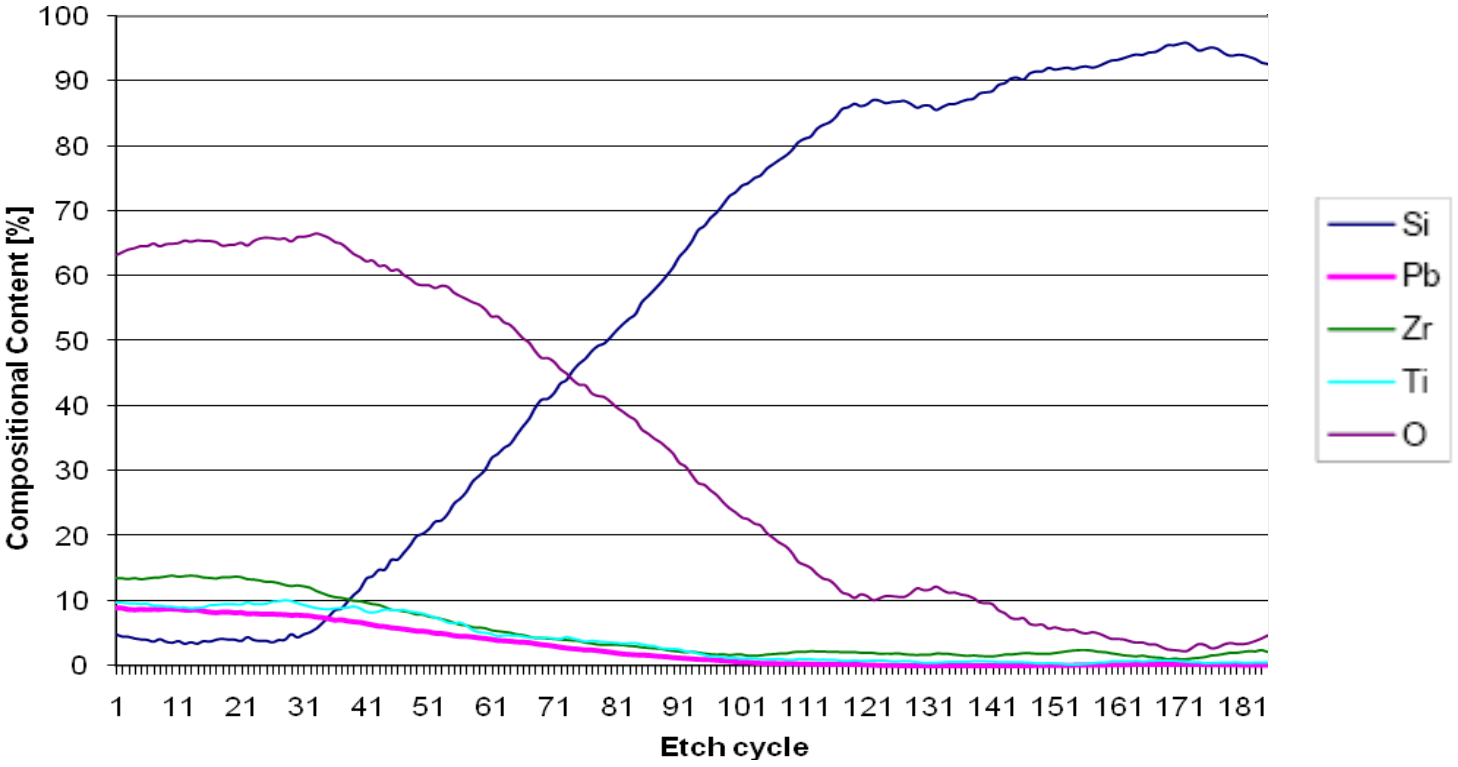

Depth profile of one layer PZT on SiO_2/Si. The interface regions are blurred.

Etching time 100 sec per step, ion current 2 kV at 0.9 µA

A triplication in etch cycles was needed to reach a comparable depth

Indication of **formation of some lead silicate** ($PbSiO_3$)

Lead Silicate or not?

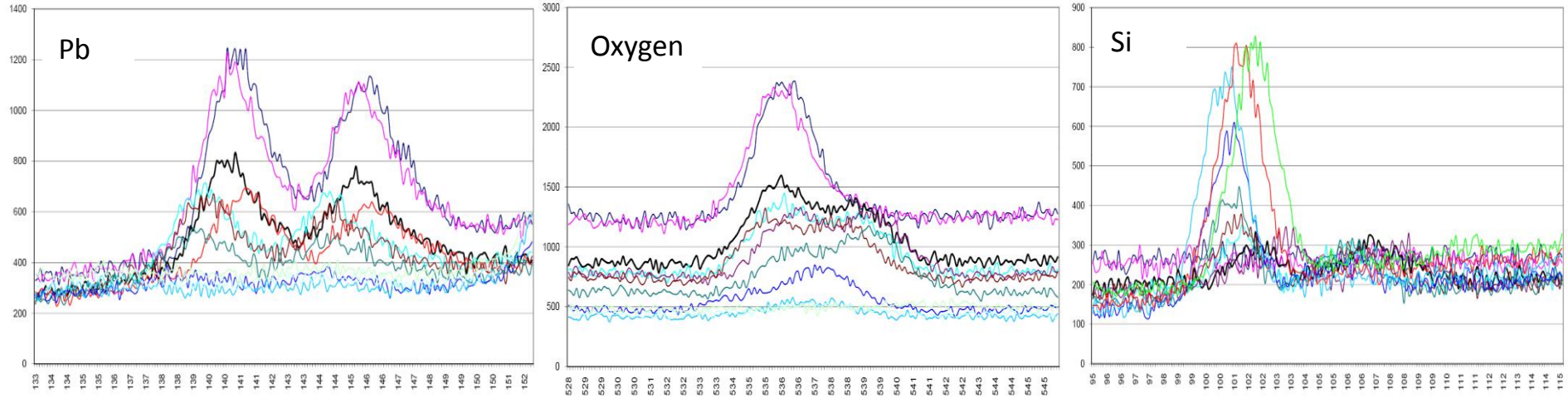

Details oft the Auger analysis for Pb, Oxygen and Si in the interfacial region of PZT on SiO2/Si. ***Black, thick trace: etch cycle 54.***

The first two traces after etch **cycles 15 and 32** (top blue and magenta in the Pb and oxygen spectra) show that Pb and oxygen are present in the expected contribution.

After etch **cycle 54** a double peak begins to appear in the oxygen and Si spectra.

The **Pb double peak** moves slightly to lower energies and begins to "wobble" around this position with increasing depth until it **vanishes after the 94th etch cycle** (second dark blue trace).

After the Pb is not traceable anymore the oxygen shows only one peak at higher energy and the Si only one at lower energy. The oxygen peak is decreasing and the Si is increasing while shifting again to a higher energies with further etch cycles.

The strong relationship between the behaviour of the Pb, oxygen and Si auger electrons confirms the assumption of **the formation of lead silicate in diffusion region**.

Summary

- **PST growths directly on top of SiO_2 and/or Si (100)**

It growths also on SiNx (not shown here)

The activation temperature is ~50°C higher than on Pt/Ti

- **Auger Analysis of PST on top of SiO_2**

Strontium diffuses slightly more into SiO_2 than Lead or Titanium

Clearly defined interfacial regions are visible

- **Auger Analysis of PZT on top of SiO_2**

All Elements of PZT diffuse into the SiO_2 layer

Interfacial regions are blurred

Strong evidence of the formation of Lead Silicate

Part III
Conclusions of this Talk

• A theoretical understanding of Ferroelectricity was given;
including: Phase Transitions in perovskite Crystals, Curie Temperature, loss mechanisms and the non-linear response of ferroelectrics (in the paraelectric state).

• The Sol-Gel Synthesis of (Ba, Sr)TiO_3 and (Pb, Sr)TiO_3 was presented.

• Problems, e.g. cracking, of BST were identified and remain unsolved.

• PST was presented as an excellent candidate for frequency agile applications.

PST Studies

• Mn B-Site Doping improves the performance significantly.

• Higher Dielectric Constant, lower Loss and enhanced Tunability with an adequate doping level.

• PST onto SiO_2, Si or SiNx without a metallic-like seeding layer is possible and well understood.

Thanks!